Development of a subject specific 3D knee finite element model to estimate the effect of weight loss on cartilage biomechanics

Julius Dahlgren

Lund, August 2022

LUND UNIVERSITY

Master's Thesis in Biomedical Engineering

Faculty of Engineering, LTH
Department of Biomedical Engineering

Supervisors: Gustavo Orozco and Hanna Isaksson

Title
Development of a subject specific 3D knee finite element model to estimate the effect of weight loss on cartilage biomechanics

Author
Julius Dahlgren

Figures
Created by the author if nothing else is indicated

Lunds Universitet
Institutionen för biomedicinsk teknik
Box 118
SE-221 00 Lund
Sverige

E-husets tryckeri
Lund 2022

Acknowledgements

I would like to thank my supervisors Gustavo and Hanna as well as the biomechanics group for the support and guidance during the thesis, the warm welcome to the group, and the opportunity to work with a subject I find interesting. I would also like to extend my gratitude to Tine Alkjær and Lauri Stenroth at the Parker institute at the University of Copenhagen for access to the CAROT trial data.

Abstract

Osteoarthritis (OA) is a common musculoskeletal disorder that degrades articular cartilage and is a leading cause of disability worldwide. Overweight has been considered a major risk factor of knee OA, and it is known that weight loss may reduce the risk of knee OA. The biomechanical mechanisms of how weight loss affects knee cartilage are however unknown. Evaluating the biomechanics of cartilage in-vivo is difficult, but an option is provided by numerical modeling of the knee joint using finite element (FE) modeling. FE modeling has proved to be effective in simulating knee joint kinematics and is therefore in this thesis proposed to estimate the effect of weight loss on cartilage biomechanics.

The first and main objective of this thesis was to estimate the effect of weight loss on knee cartilage biomechanics using a subject-specific FE knee joint model. The second objective was to investigate if modeling bone as a deformable, isotropic, and heterogeneous material would affect the cartilage biomechanics. The third objective was to investigate if the addition of a subchondral bone cyst (SBC), a common symptom of knee OA, in the tibia of the FE model would affect the biomechanics of cartilage and bone.

To achieve these objectives, a 3D model of a knee was manually segmented from magnetic resonance imaging (MRI) data of a participant in a weight loss focused clinical trial. The knee segmentation was meshed into a set of four different FE models and simulated using subject-specific motion analysis data for three sets of weight during the stance phase of gait.

The results of the FE analysis showed that as the subjects weight decreased from 85 kg to 74 kg, contact pressure, Von Mises stress, and maximum principal strain at the surface of the tibial cartilage decreased by 6.2 %, 6.9 %, and 6.5 % respectively at peak load during the stance phase of gait. Modeling the tibial bone as heterogeneous and deformable led to a 10.7 % and 14.8 % reduction of Von Mises stress and maximum

principal strain in the tibial cartilage when compared to rigid bone. The addition of a SBC led to a marginal decrease in contact pressure, Von Mises stress, and maximum principal strain in the tibial cartilage, but an increase in minimum principal stress and strain in the tibial bone.

In conclusion, this thesis has shown that weight loss simulated by FE analysis leads to a quantifiable reduction of the biomechanical load on knee tissues. Modeling bone as rigid also proved to be an effective simplification to reduce computational time while maintaining accuracy in the cartilage mechanics.

Further refinement of the models investigated in this thesis, for example by the addition of ligaments or more complex material models, may in the future provide an effective means of predicting cartilage response to weight loss. This could result in a clinically viable computational method of suggesting the best possible preventative treatment of OA.

List of acronyms & abbreviations

ACL - anterior cruciate ligament

BLOKS - Boston Leeds osteoarthritis knee score

CAROT - Influence of Weight Loss or Exercise in Cartilage in Obese Knee Osteoarthritis Patients Trial

CNN - convolutional neural network

DL - deep learning

FE - finite element

FEM - finite element method

GDP - gross domestic product

MRI - magnetic resonance imaging

NMV - net magnetization vector

OA - osteoarthritis

SBC - subchondral bone cyst

TE - echo time

TKR - total knee replacement

TR - repetition time

VAS - visual analog scale

Contents

Chapter 1

Introduction

Osteoarthritis (OA) is a common musculoskeletal disease affecting large parts of the global population. In the US, 10 % of men and 13 % of women over the age of 60 have knee OA, a figure that is increasing every year due to an aging population, obesity, and traumatic injuries [1]. The cost of OA to healthcare systems and society as a whole is large, while the disease is difficult to prevent [2]. The disease is characterized by the degradation of articular cartilage, and the progression of OA may be accelerated by abnormal joint loading due to traumatic injury or obesity. Obesity is a major risk factor for knee OA, increasing the risk by five times in men and four times in women when compared to normal-weight men and women [3]. It is known that weight loss can reduce the risk of knee OA [4], but it is not known how weight loss mechanically affects the knee cartilage. Answering this question is problematic, since evaluating the mechanics of cartilage in-vivo poses a risk of damage to the joint. Imaging methods such as radiography and magnetic resonance imaging (MRI) can only be used to investigate very simplified mechanical properties of cartilage [5]. A solution to this problem is found in numerical modeling of the knee joint using finite element (FE) analysis.

FE analysis of the mechanical behavior of human anatomy was at its inception applied in structural analysis of bone [6]. Since then, the application of FE analysis on the musculoskeletal system has broadened to include fracture risk assessment, prosthetic design, and modeling of soft tissues such as cartilage [7]. The kinematics of the knee joint and cartilage have been investigated using FE analysis in several studies, using different material models, geometry, and input data for the simulation [8, 9, 10, 11, 12]. By proposing mechanobiological algorithms,

studies have also attempted to model the progression of OA [2]. The effect of weight loss on the biomechanics of cartilage, menisci, and bone using subject-specific geometry and gait data have however yet to be investigated. This is of interest to acquire a better understanding of how weight loss affects cartilage, bone, and the risk of OA.

1.1 Aim

The purpose of this thesis was to estimate the effects of weight loss on cartilage biomechanics in a patient specific manner by developing a 3D finite element model of the knee.

The main question to be answered was:

- What will the biomechanical response of the knee joint cartilage-bone unit be after weight loss simulated by FEM?

The secondary objectives of the thesis were:

- Would modeling the tibial bone as a deformable, isotropic heterogeneous material affect the biomechanics of the cartilage?
- How would the inclusion of a subchondral bone cyst (SBC), a common symptom of OA, in the tibial bone of the FE model affect the biomechanics of cartilage and bone?

The main hypothesis was that stresses, strains, and contact pressure in the cartilage would decrease as body weight is reduced. It was also hypothesized that when modeling bone as an isotropic homogeneous solid, treating the bone as rigid (non-deformable) in the simulation would be a suitable simplification that could save computation time.

1.1.1 Design of the study

To meet these objectives, knee MRI data of one subject participating in a research trial was obtained in collaboration with the University of Copenhagen [13]. A 3D model of the knee was first created from the MRI data by segmentation of cartilage, menisci, and bone. Four different FE models implementing rigid bone, deformable bone, heterogeneous bone as well as heterogeneous bone incorporating a SBC would then be developed by meshing the segmented geometry. These models

were then simulated for the stance phase of gait using subject-specific body weight and gait data acquired in the research trial. This methodology is described in Figure 1.1.

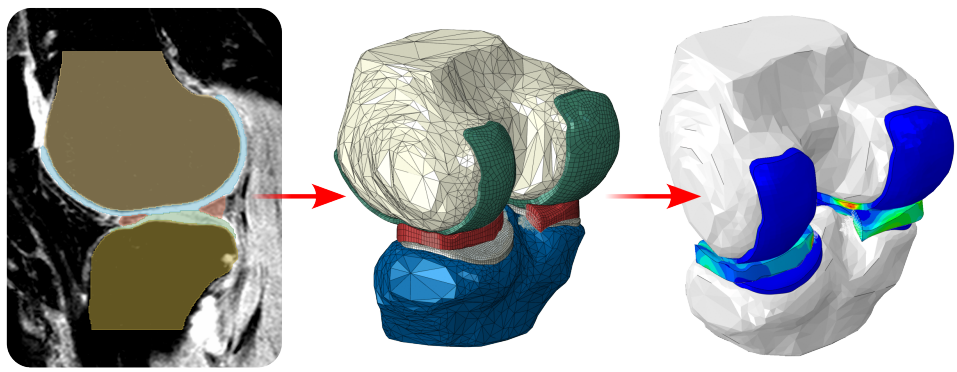

Figure 1.1: The general methodology of producing and simulating the 3D FE knee models in this thesis.

Chapter 2

Background

2.1 The knee

2.1.1 Anatomical directions

A guide to the anatomical directions and axes referred to throughout this thesis is presented in Figure 2.1.

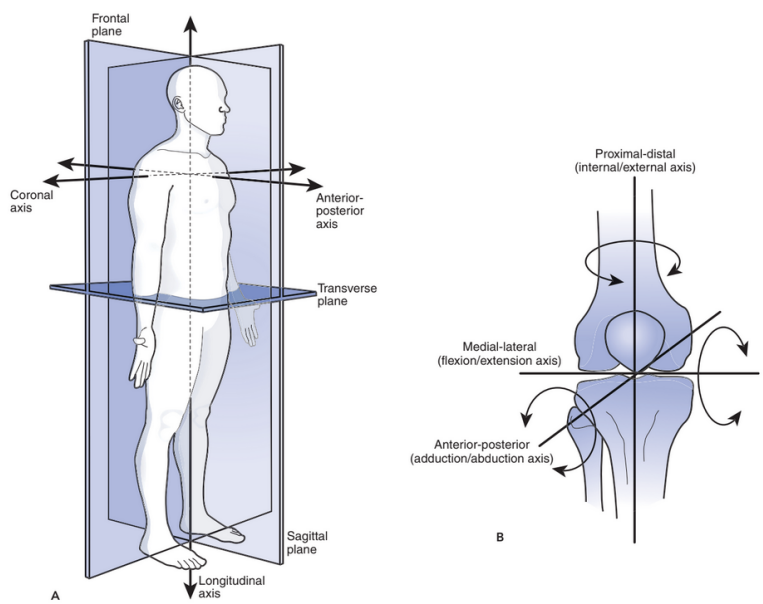

Figure 2.1: A) The anatomical planes. B) The six degrees of freedom of the knee [14].

2.1.2 Anatomy of the knee

The knee is the largest joint of the body and consists of two separate joints, the tibiofemoral and the patellofemoral joint. It serves as the hinge between the two largest lever arms of the body and therefore sustains large forces and moments. Several muscles generate forces over the knee joint, but the largest part of these originate from the quadriceps. To manage these forces and facilitate locomotion, the knee includes several ligaments that assist in stabilizing and restricting the possible range of motion of the joint, seen in Figure 2.2. The number of connective tissues critical to the function of the joint combined with the large forces it transmits makes the knee particularly susceptible to injury [14].

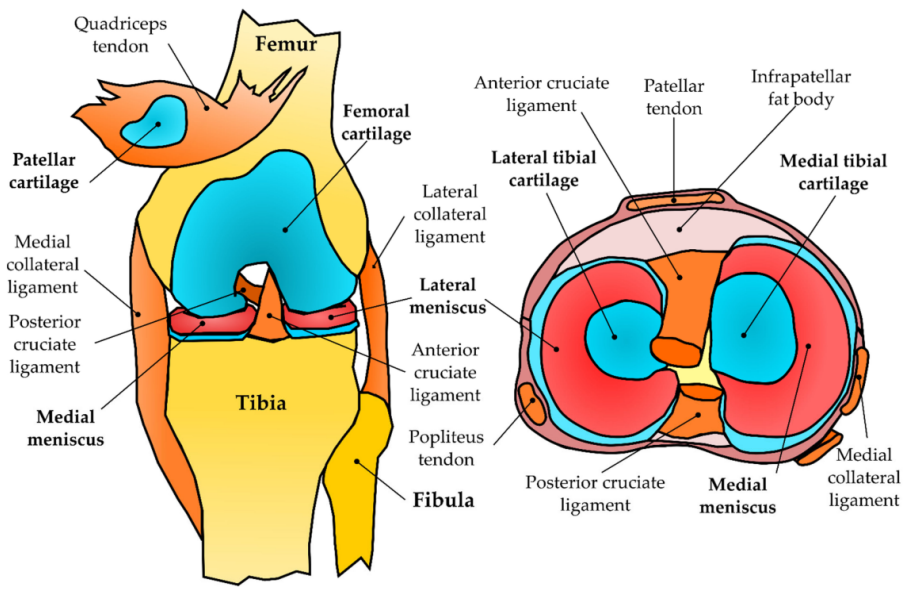

Figure 2.2: A schematic of knee joint anatomy [12].

2.1.3 Biomechanics of the knee

The knee joint is capable of motion in six degrees of freedom. The greatest amount of motion is found in the sagittal plane where flexion and extension of the knee typically permit 3° of extension to 155° of flexion [14]. The range of flexion is usually limited by the calf coming into contact with the thigh while the range of extension is limited by the collateral and cruciate ligaments. Motion of the knee in the frontal plane (abduction and adduction) is comparatively small and restricted

by the collateral ligaments and the current degree of flexion in the knee. Motion in the transverse plane (internal and external rotation) is small as well and is restricted by the ligaments, the meniscii, and interlocking of the femoral condyles with the tibia at different angles of flexion. Translation of the tibia in relation to the femur does occur to a small degree during physical activity but is highly restricted by the ligaments [14].

2.2 Articular cartilage

Articular cartilage (or hyaline cartilage) is found in the freely movable synovial joints of the body, such as the knee, hip, and elbow. It is a tissue made up of cells known as chondrocytes in a matrix of several components [15]. The composition of articular cartilage is 70-85 % water while the remainder consists primarily of proteoglycans and type II collagen. Of the solid components, collagen makes up 60-70 % of the tissue while proteoglycans make up around 30 %. The structure of these components and the interaction between them are what determine the mechanical properties of the tissue [16]. Articular cartilage is divided into four zones: the superficial zone, the middle zone, the deep zone, and the calcified zone (see Figure 2.3). In the deep zone, collagen fibers are oriented perpendicular to the surface and packed in bundles. In the upper deep zone and the middle zone, the orientation of the collagen fibers begins to diverge, forming a network around the chondrocytes. In the superficial zone, collagen fibers form layers oriented tangentially to the surface. The interaction between the charged proteoglycans in the cartilage contributes to the compressive stiffness of the tissue. Proteoglycans are macromolecules composed of negatively charged molecules called glycosaminoglycans (chondroitin sulfate and keratan sulfate) attached to a protein chain [17]. Proteoglycans attach in turn to the molecular chain of hyaluronic acid, forming a proteoglycan aggregate. The high number of charges on the aggregate makes the molecule spread out and occupy a large volume in an aqueous solution. Proteoglycan content varies throughout the depth of articular cartilage and is highest below the calcified zone near the subchondral bone. The distribution of water in cartilage is reversed to that of proteoglycans, being highest in the superficial zone and lowest in the calcified zone [16].

Because the mechanical behavior of cartilage is dependent on the fluid as well as solid components of the tissue, it has been described

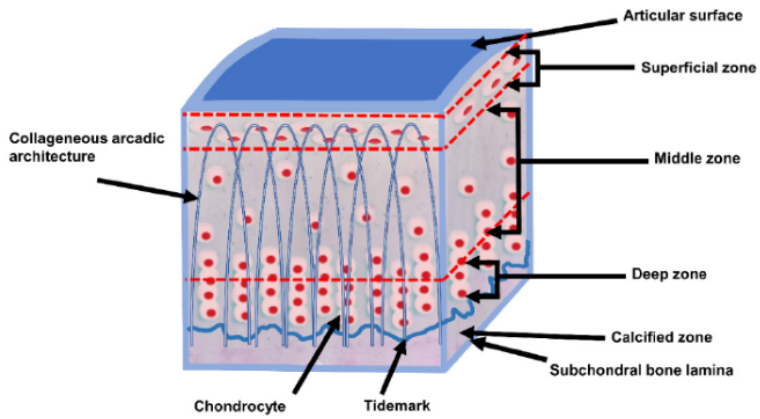

Figure 2.3: Cross-section of articular cartilage depicting the structure of the tissue [15].

using a biphasic model. This model puts the solid components of the tissue (collagen, proteoglycans, cells, and lipids) into one phase and the interstitial fluid of the cartilage in the other [15]. As cartilage is deformed, fluid flows through the tissue and the articular surface. For high loading rates or impact scenarios, cartilage usually behaves as a single-phase incompressible elastic material as there is not enough time for the fluid to flow. In mechanical experiments or numerical modeling, several material models of cartilage exist that more accurately take into account one or more properties of the tissue [12]. The balance between the solid components and the water content of cartilage is a major determining factor of its mechanical properties. As glycosaminoglycan content decreases, the compressive stiffness of the tissue decreases. As water content increases, compressive stiffness further decreases while the permeability of the tissue increases, allowing for a higher rate of deformation [16]. These relations may help understand the mechanical mode of failure of cartilage and how tissue degeneration such as OA develops in the knee joint.

2.3 Osteoarthritis

Osteoarthritis (OA) is one of the most common joint disorders and a leading cause of disability in the developed world. The impact of OA on healthcare systems is high due to the cost and complexity of treatment. For example in the US, the cost of medical care and earning

losses attributable to OA was 1 % of GDP in 2013 and may be as high as 2.5 % in some countries [18, 19]. This figure is likely to rise due to an aging population and increasing prevalence of obesity [1]. The majority of costs associated with OA treatment are due to total knee replacement surgery (TKR) [19]. Demand for TKR in the US is expected to increase by more than 600 % by 2030 [20], with a current estimate of approximately 600 000 TKR procedures taking place annually [21].

The early stages of OA is characterized by fibrillation (fraying of the collagen fibers) and cracking of the articular surface. Degradation of the tissue may then proceed undetected for years until the main symptoms of joint pain and limited range of motion present themselves. Since cartilage is an aneural tissue, it is not possible for an individual to sense onset of the condition. Therefore it is difficult to detect OA before damage to the cartilage has occurred. Because blood supply and nutrient exchange to cartilage is limited, its ability to heal is limited as well.

There are several factors that increase susceptibility to OA. Systemic ones include for example age, perhaps the most prominent risk factor, as well as sex and genetics. The more direct factors are obesity, joint injury, joint deformity, muscle weakness, and long-term sporting [1]. An injury to the anterior cruciate ligament (ACL) for example does not directly affect the cartilage but leads to local alterations of the loading conditions in the knee joint and subsequent initiation of damage to the cartilage. Similarly, alterations in gait due to pain avoidance can also be an initiator of OA in the knee. Studies have also shown that excessive loading rate applied to cartilage is the main initiator of OA, for example in impulse loading scenarios, rather than the magnitude of the load [22, 16]. Diagnosis of OA is usually confirmed by patient history and examination combined with radiography or magnetic resonance imaging (MRI) to reveal the extent of damage to the cartilage.

2.4 Magnetic resonance imaging

Medical imaging systems have found a central role in diagnosis of OA and determining the state of cartilage. The Kellgren-Lawrence system is one of the more common classification systems based on imaging data. It utilizes X-ray imaging to classify OA in grades of 0-4 in terms of progression of the condition. The disadvantage of using radiography to image cartilage is that X-rays are attenuated minimally by the tissue,

which is mostly composed of water. Cartilage therefore produces low if any contrast in radiography images, making it indistinguishable from other tissues. This is why the Kellgren-Lawrence system relies on detecting osteophytes, bony protrusions commonly seen in arthritic cartilage, to determine the state of the tissue [23]. In contrast to radiography, MRI is an excellent tool to image cartilage since it detects the magnetic field of hydrogen atoms in the water of the cartilage, producing clear images of the tissue.

As a radiofrequency pulse is emitted to the tissue in the magnetic field of an MRI scanner, the net magnetization vector (NMV) of hydrogen nuclei in the tissue flips from the plane of the magnetic field to the transverse plane, while the spinning hydrogen nuclei are all exactly in phase. The time it takes for the NMV to realign with the equilibrium field emitted by the scanner and the time it takes for the spinning nuclei to dephase are referred to as longitudinal relaxation (T1) and transverse relaxation (T2) respectively [24, 25].

A number of different MR sequences are used to image cartilage. These vary in terms of parameters such as repetition time (TR) and echo time (TE), resulting in different T1 and T2 times, producing different contrast between cartilage and surrounding tissues [26]. The imaging resolution of an MRI system is highly dependent on the strength if the magnetic field it generates. The stronger the magnetic field, the higher the resolution, facilitating production of higher quality 3D models of cartilage and the knee joint.

2.5 Segmentation

Image segmentation is the process of generating discrete groups of pixels in an image that belong to specific objects. In medical applications, segmentation is usually performed manually, semi-automatically, or by fully automatic methods [20]. Manual methods (or interactive methods) rely on directly delineating the relevant tissues or objects in an image stack using image processing software. For medical image volumes, this can be successful, but is highly dependent on the operator and is labor-intensive as a rule. Therefore it is discouraged in many situations. Semi-automatic methods make use of more conventional methods of image processing such as separating tissues based on properties such as pixel intensity and intensity gradients (edges in the image) [20]. This can produce segments more effectively, but depending on the image

quality, the segments may overlap with multiple tissues due to poor contrast. This usually requires manual correction of the segmentation. Fully automatic methods include ones based on deep learning (DL), such as convolutional neural networks (CNN). These have recently achieved high accuracy in segmenting medical image data and can drastically reduce the amount of time needed to produce a segment. Accurate segmentation is critical in establishing subject-specific anatomic models and can independently be applied in the diagnosis of knee OA [20].

2.6 The finite element method

The finite element method (FEM) is one of the primary tools used to simulate the mechanical behavior of materials and structures. Physical phenomena such as those encountered in mechanics are described by differential equations. Solving differential equations for complex geometries using analytical methods is generally impossible. FEM tackles this issue by converting the analytical problem into a numerical one that is solved computationally. The numerical solution is not exact, but approximate [27]. Depending on the level of detail of the FE mesh, the numerical solution converges toward the exact solution. FEM is applicable not only for mechanical problems but on a range of physical phenomena described by differential equations. The FE formulation of a problem is obtained by first establishing what is known as the strong form. This is followed by acquiring the weak form of the problem, making an elementwise approximation over the body of the unknown function, and then choosing the weight function by the Galerkin method. For a linear, one-dimensional mechanical problem, this results in an equation on the form

$$\left(\int_a^b \boldsymbol{B}^T AE\boldsymbol{B} dx \right) \boldsymbol{a} = -[\boldsymbol{N}^T A\epsilon]_a^b + \int_a^b \boldsymbol{N}^T b dx \tag{2.1}$$

where A is the cross sectional area of the object, E is Young's modulus, ϵ the strain, b the body forces, $\boldsymbol{a}$ are the nodal displacements, $\boldsymbol{N}$ is the global shape function matrix and $\boldsymbol{B} = \frac{d\boldsymbol{N}}{dx}$. We now define the matrices

$$\boldsymbol{K} = \int_a^b \boldsymbol{B}^T A E \boldsymbol{B} dx \tag{2.2}$$

$$\boldsymbol{f}_b = -[\boldsymbol{N}^T A \epsilon]_a^b \tag{2.3}$$

$$\boldsymbol{f}_l = \int_a^b \boldsymbol{N}^T b dx \tag{2.4}$$

where $\boldsymbol{K}$ is the stiffness matrix, $\boldsymbol{f}_b$ is the boundary vector and $\boldsymbol{f}_l$ is the load vector. Equation 2.1 can now be compactly written as

$$\boldsymbol{K}\boldsymbol{a} = \boldsymbol{f}_b + \boldsymbol{f}_l \tag{2.5}$$

If we further define the vector

$$\boldsymbol{f} = \boldsymbol{f}_b + \boldsymbol{f}_l \tag{2.6}$$

where $\boldsymbol{f}$ is the force vector, we obtain

$$\boldsymbol{K}\boldsymbol{a} = \boldsymbol{f} \tag{2.7}$$

where $\boldsymbol{K}$ is the stiffness matrix, $\boldsymbol{a}$ is the nodal displacement vector and $\boldsymbol{f}$ is the force vector describing the boundary conditions of the problem. The solution to (2.7) is either displacement controlled where the nodal displacements in $\boldsymbol{a}$ are known and the equation can be solved directly, or load controlled where $\boldsymbol{f}$ is known and $\boldsymbol{K}$ must be inverted to obtain the nodal displacements. For more detailed derivations of the FE formulation, the reader is referred to relevant literature [27].

2.6.1 Non-linear finite element method

In the case of non-linear problems, the numerical solution is more complex. In a materially linear problem, the stiffness matrix $\boldsymbol{K}$ only needs to be calculated once to obtain the nodal forces or displacements in question. For a non-linear problem, force or displacement is applied in increments while $\boldsymbol{K}$ may need to be continually re-calculated using a numerical algorithm in order to obtain a solution in equilibrium. One widely used algorithm for solving non-linear problems is the Newton-Raphson method. The Newton-Raphson method advances the numerical solution iteratively until an equilibrium condition between the internal and external forces acting on the nodes of an element is fulfilled.

For a load controlled problem with several degrees of freedom, we start in a known state of displacement $\boldsymbol{a}$ denoted by the superscript i

$$\boldsymbol{K}_t^{(i)} \Delta \boldsymbol{a} = -\boldsymbol{r}(\boldsymbol{a}^{(i)}) \tag{2.8}$$

where $\boldsymbol{K}_t$ is the tangent stiffness, $\Delta \boldsymbol{a}$ the iterative displacement increment, and $\boldsymbol{r}$ is the residual given by

$$\boldsymbol{r}(\boldsymbol{a}) = \boldsymbol{f}_{int}(\boldsymbol{a}) - \boldsymbol{f}_{ext} = 0 \tag{2.9}$$

where the external force is assumed to be independent of the displacement. Solving (2.8) for $\Delta \boldsymbol{a}$ provides the next state of nodal displacement $i + 1$

$$\boldsymbol{a}^{(i+1)} = \boldsymbol{a}^{(i)} + \Delta \boldsymbol{a} \tag{2.10}$$

This algorithm continues to incrementally increase the displacement until the equilibrium defined by the residual (2.9) is small enough and the current state of displacement $\boldsymbol{a}^{(i)}$ is accepted. Solving non-linear systems is more computationally expensive than linear systems, taking many times longer to solve. As many tissues of the knee exhibit non-linear behavior, both in terms of constitutive relation and structure, the Newton-Raphson method is a suitable solution for the models investigated in this thesis. For more details regarding derivations of the Newton-Raphson method, the reader is referred to relevant literature [28, 29].

2.6.2 Finite element meshing

For FE analysis of the knee joint, the segmented anatomy must be discretized into a mesh of polyhedral elements. Meshing using tetrahedral or hexahedral elements are two of the most common approaches (see Figure 2.4). Automatic tetrahedral meshing algorithms are used in several commercial programs. They are robust and capable of meshing arbitrary geometries and are therefore suitable for complex anatomical geometry. In contrast, hexahedral meshing is more difficult to achieve for complex geometries since most commercial tools are built around meshing engineering components with more regular structure [7]. Currently, only one option for automatic hexahedral meshing of knee cartilage structures exists in literature [30]. Hexahedral elements are however

the preferred option in many cases, as the volume of one hexahedral element must be represented by at least five tetrahedral elements, resulting in a model that is more expensive in terms of computation time [7]. In addition to this, tetrahedral meshes may produce acceptable results for the prediction of displacements but are less accurate when predicting stresses [30].

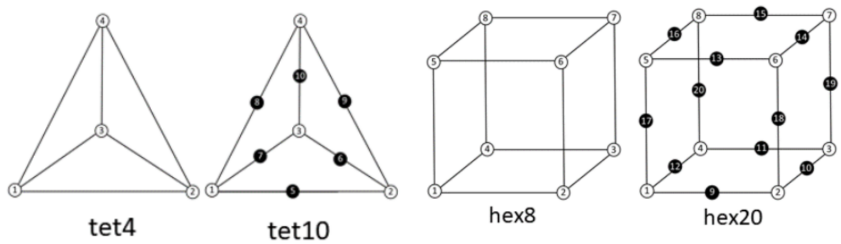

Figure 2.4: Linear (tet4, hex8) and quadratic (tet10, hex20) tetrahedral and hexahedral elements. [31]

Chapter 3

Materials & Methods

3.1 Overview

The main work of establishing the FE models in this thesis can be divided into three stages, presented in Figure 3.1. The first was pre-processing, where the knee joint was segmented from MRI data and a finite element mesh of the segments was generated. The second was processing, where the models were simulated for subject specific weight and gait data in Abaqus (Dassault Systémes Simulia Corp., Providence, RI, USA). The third was post-processing, where the results of the simulations were compiled and analyzed.

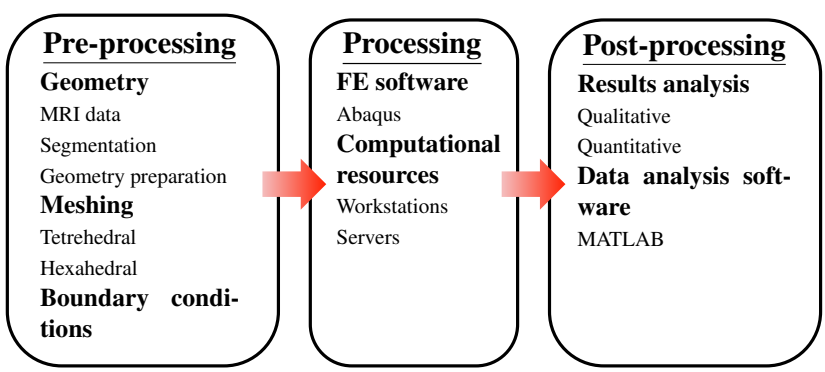

Figure 3.1: The general workflow of establishing and analysing the FE models of the knee.

3.2 Materials

The knee models in this thesis were created from a set of MR images of the left knee of a 62 year old female participant in the study Influence of Weight Loss or Exercise on Cartilage in Obese Knee Osteoarthritis Patients Trial (CAROT) [13], performed at the Department of Rheumatology, Frederiksberg Hospital, Denmark, and obtained in collaboration with the University of Copenhagen. The CAROT trial examined obese patients with knee OA and how their condition changed after 16 weeks of intense weight loss followed up by one year of either dietary support, exercise, or no support (control group). The subject examined in this thesis was in the group that received one year of dietary support. Weight data for the subject at three time points: baseline (85 kg), 16 weeks (74 kg), and 68 weeks (72 kg), and subject-specific gait data captured only at baseline weight were also obtained from the CAROT trial. The MR images were only of the knee at baseline weight. Participants in the study gave written informed consent, which was approved by the ethics committee of the Capital Region of Denmark [H-B-2007-088]. The MR images were acquired using a Philips Medical Systems Intera 1.5 Tesla MRI system. The imaging sequence used was Sagittal 3D FLASH gradient-echo (repetition time = 21 ms, echo time = 3.5 ms, slice thickness = 3 mm, flip angle = 20°, reconstructed image size = 512x512 pixels, number of slices = 80, voxel resolution = 0.3125x0.3125x1.5 mm) [32].

3.2.1 Subject specific gait data

Subject-specific reaction force and flexion-extension angle measured at the knee during stance phase of the gait cycle was acquired in the CAROT study using a motion analysis system and a musculoskeletal model developed in OpenSim [32]. The data was shared by the University of Copenhagen and was not produced by the author. Knee axial force and flexion-extension angle throughout the gait cycle (see Figure 3.2) were acquired from this model at baseline weight (85 kg) and used as the input conditions in the FE models. The knee axial force at 16 and 68 weeks was obtained by scaling the baseline axial force by a factor of 0.8706 for 16 weeks and a factor of 0.8470 for 68 weeks.

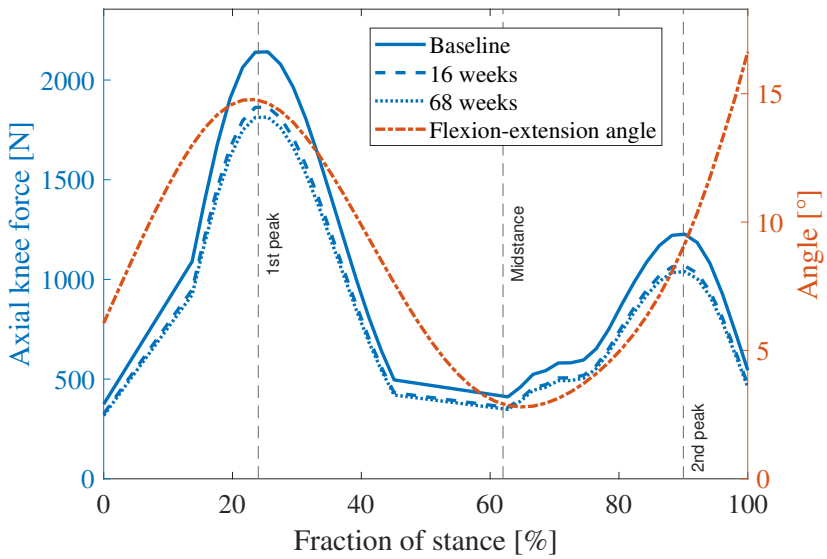

Figure 3.2: Subject specific axial contact force and flexion-extension angle acquired in the CAROT study.

3.2.2 Material models

The choice of material properties used in the models was based on a literature review of properties used in numerical models of the tibiofemoral joint by Peters et al. [33], as well as other studies specified in Table 3.1. Bone, menisci, and the cyst were modeled as homogeneous, isotropic linear elastic materials, while cartilage was modeled as a homogeneous, isotropic, Neo-Hookean hyperelastic material.

The hyperelastic parameters C_{10} and D_1 used in the Neo-Hookean material definition in Abaqus [38] were calculated using equations

$$C_{10} = \frac{\mu_0}{2} \tag{3.1}$$

and

$$D_1 = \frac{3(1-2\nu)}{\mu_0(1+\nu)} \tag{3.2}$$

where μ_0 is the initial shear modulus and it was assumed that $\mu_0 = G$.

Table 3.1: Material properties used in the models. E is Young's modulus, ν is Poisson's ratio and G is the shear modulus.

Model	Parameters	References
Cortical bone	E = 17 GPa, $\nu = 0.3$	Andersson et al. 2008 [34] Peters et al. 2018 [33]
Subchondral bone	E = 3 GPa, $\nu = 0.3$	Choi et al. 1990 [35]
Trabecular bone	E = 160 MPa, $\nu = 0.3$	Behrens, Walker & Shoji 1974 [36]
Cyst wall	E = 12 MPa, $\nu = 0.45$	Sarrafpour et al. 2019 [37]
Menisci	E = 20 MPa, $\nu = 0.3$	Mononen et al. 2016 [2]
Cartilage	G = 6.8 MPa, $\nu = 0.45$	Andersson et al. 2008 [34] Peters et al. 2018 [33]

3.3 Development of the finite element models

3.3.1 Pre-processing

The first stage of developing the FE knee model was pre-processing, where an FE mesh of the knee was created from MRI data (see Figure 3.3).

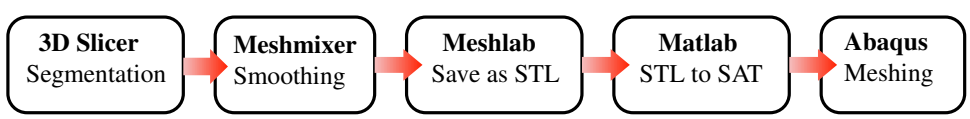

Figure 3.3: The workflow of the meshing process.

Segmentation of the knee joint

The femoral bone, femoral cartilage, menisci, tibial cartilage and tibial bone of the model were segmented manually from the MRI data using the open source software 3D Slicer. The segmentation was performed by the author and was verified by the supervisor at the Department of Biomedical Engineering at Lund University. The segmentation was performed in the sagittal view of the MR data (see Figure 3.4) as the other views provided lower resolution, less accurate segmentation, and greater difficulty in discerning the tissues of the knee. The contrast

and brightness of the image were adjusted differently when segmenting cartilage, menisci and bone to improve discernibility of the tissues. Five segmented volumes representing the femur, femoral cartilage, menisci, tibial cartilage and tibia were exported from 3D Slicer.

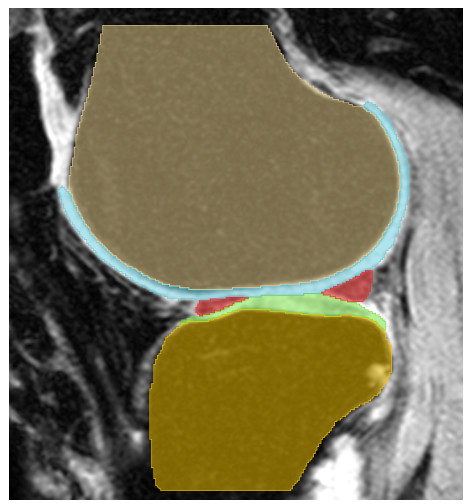

Figure 3.4: A segmented slice of the MR data in the sagittal plane. Light yellow depicts the femur, blue the femoral cartilage, red the menisci, green the tibial cartilage and dark yellow the tibia.

Meshing

The first stage of producing a mesh of the knee joint segments was performed in Meshmixer (Autodesk Inc, San Rafael, CA, USA). Objects unconnected to the main segment were first removed. The segments were then made solid using the maximum value of solid accuracy to preserve as much as possible of the original segmented volume. The triangle count of the mesh was then reduced using shape preservation to approximately 1 500 triangles for the femoral and tibial bone, while the femoral cartilage, tibial cartilage and menisci were reduced to approximately 30 000 triangles. The segments were subsequently smoothed using a smoothing factor of 0.5, a smoothing scale of 2 and shape preservation (see Figure 3.5).

The smoothed segments were imported from Meshmixer into Meshlab and then re-exported as STL files. The purpose of this was to avoid an error when importing STL files from Meshmixer into Abaqus. To enable meshing of the segments in Abaqus, the STL files generated in

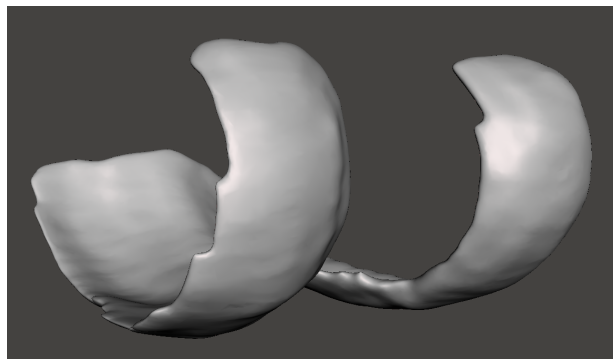

Figure 3.5: The smoothed femoral cartilage segment

Meshmixer were converted into the SAT format using a Matlab-script [39].

The femoral cartilage, tibial cartilage and menisci were meshed in Abaqus according to a guide by Bolcos [40]. For the femoral cartilage, two datum planes were defined from which the edges of the femoral cartilage geometry was cut using the Create Cut: Extrude option in the Part module. The purpose of this was to create a regular edge along the geometry of the cartilage that enabled hexahedral meshing. This meant that a part of the segmented 3D volume of the cartilage was removed, a simplification of the geometry deemed acceptable as the loss of segmented cartilage volume would not drastically affect the outcome of the simulation. The surface mesh generated in Meshmixer was removed by using Virtual Topology: Combine Faces in the Mesh module. The subchondral surface of the femoral cartilage was combined into one face, while the edge surface and cartilage surface were combined into respective faces.

For the tibial cartilage, a single datum plane was defined from which a single cut was made to obtain a regular edge. The surface mesh was then removed by combining the cartilage surface, edge surface and subchondral surface into separate faces.

The edges of the menisci and parts of the segmented volume corresponding to the meniscal horns were cut as well.

Using the tool Partition Cell: Use Datum Plane, the segments were partitioned into cells to further facilitate hexahedral meshing. The femoral cartilage was partitioned into 12 cells (see Figure 3.6), the medial tibial cartilage into 12 cells, the lateral tibial cartilage into 10 cells, the medial meniscus into 6 cells and the lateral meniscus into 10 cells.

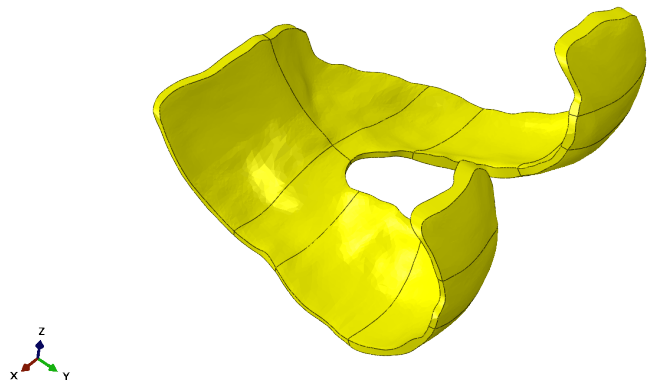

Figure 3.6: Cut and partitioned femoral cartilage.

Following Mononen et al. [2], to achieve good contact convergence, seeding of the femoral cartilage was done using a global element size of approximately 1.5 mm, while the menisci and tibial cartilage had an element size of approximately 1.0 mm and 0.7 mm respectively. These tissues were also assigned 3 depth-wise element layers with separate edge seeds. The tissues had an edge seed bias ratio of 1.5 and 3 for the femoral and tibial cartilage respectively in the direction of respective cartilage surface, while the menisci had no edge seed bias. For the menisci, the number of elements allowed for non-depthwise edges were manually limited to between 4 and 20 elements to enable meshing of the part.

In Mesh Controls, the soft tissues were assigned the Hex element type (C3D8) using the Sweep mesh technique. 7 728, 13 155 and 4 836 elements were generated for the femoral cartilage, tibial cartilage and menisci respectively.

Meshing the homogeneous bone models

When meshing the femoral and tibial bone, the surface mesh generated in Meshmixer was kept when the SAT-files were imported into Abaqus. For the homogeneous bone models, the parts were meshed without any partitions using quadratic tetrahedral elements (C3D10). The femoral and tibial bone was assigned an approximate element size of 20 mm and meshed using the Free meshing technique in Mesh Controls. The femoral mesh consisted of 16 758 elements while the tibial mesh consisted of 13

692 elements. The complete knee mesh of 56169 elements can be seen in Figure 3.7.

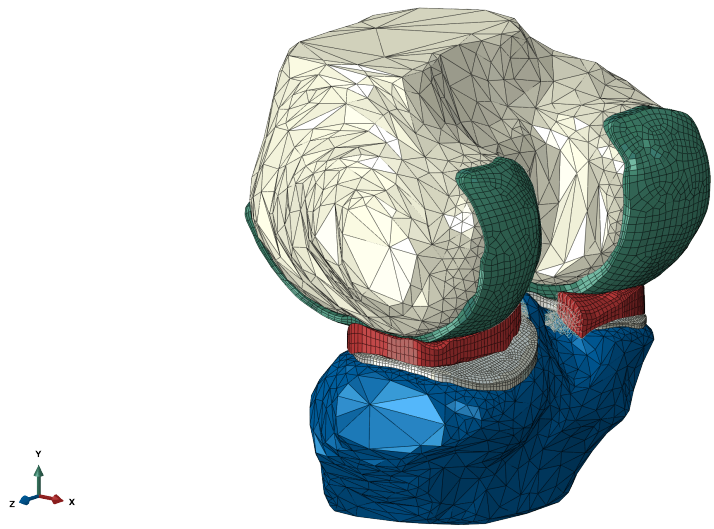

Figure 3.7: Mesh of the complete knee segmentation.

Meshing the heterogeneous bone model

To investigate if modeling bone as deformable and heterogeneous would have any effect on cartilage biomechanics, a heterogeneous tibia model was created, incorporating cortical, trabecular and subchondral bone. A copy of the smoothed tibia segment was made in Meshmixer. The volume of the copy was scaled by a factor of 0.95 in the Transform module. The scaled model was then imported into Abaqus and the same assembly as the original tibia model. The original tibia was given a section assignment and material model corresponding to cortical bone while the scaled tibia was assigned a section using a trabecular bone material model. The models were then combined using Merge in the assembly module to produce a part with an outer shell of cortical bone approximately 1.5 mm thick, and an inner section of trabecular bone. A single datum plane was defined approximately 1 mm below the tibial plateau from which the part was partitioned. The resulting proximal partition above the datum plane was assigned a material model for subchondral bone, while the distal partition below retained the cortical bone model. The resulting subchondral bone section was approximately

1 mm thick. Keeping the surface mesh from Meshmixer, the model was then assigned an approximate element of size of 3 mm and meshed using quadratic tetrahedral elements (C3D10), resulting in a mesh consisting of 44 882 elements.

The subchondral bone cyst model

To investigate a hypothetical scenario where the subject had a subchondral bone cyst (SBC) and how it would affect the biomechanics of the cartilage, another tibia model was created. A solid sphere part with a diameter of 6 mm representing the cyst was created. This sphere was assigned a material section corresponding to cyst wall and merged into the heterogeneous tibia model. The SBC was placed centrally in the medial tibial compartment, approximately 1 mm below the subchondral bone plate. The position and dimension of the SBC was consistent with clinical observations of position, size, and distance from the joint line of SBC's in the tibia [41]. The SBC was assigned an approximate element size of 0.6 mm while the rest of the tibia kept an element size of 3 mm. The part was meshed tetrahedrally (C3D10) resulting in a mesh of 59 309 elements. A comparison of the mesh between the heterogeneous and SBC tibia models can be seen in Figure 3.8.

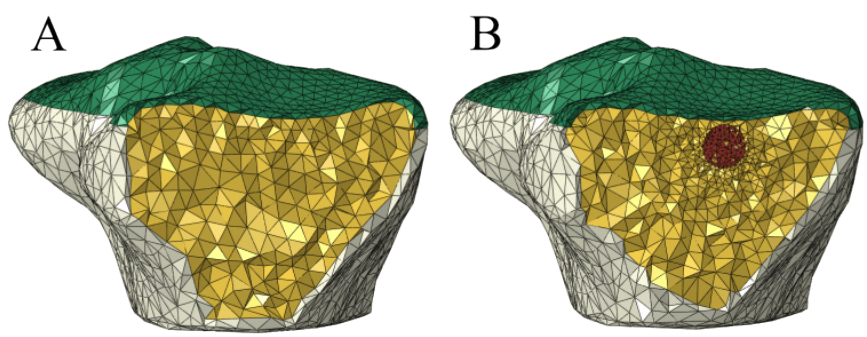

Figure 3.8: Cross section of **A**) the meshed heterogeneous tibia model **B**) the meshed SBC tibia model.

3.3.2 Processing

Assembly

The meshed knee parts were rotated in the Assembly module to make the longitudinal axis of the parts correspond to the Y-axis, the coronal axis to the Z-axis and the anterior-posterior axis to the X-axis. An internal rotation of five degrees was applied to the femur and femoral cartilage to improve contact with the tibial cartilage. To prevent initial overlap between the parts, tibia and tibial cartilage was translated 2.5 mm in the negative Y-direction while the menisci were translated 2.0 mm in the same direction. The menisci were attached to the tibia by using linear springs connecting the nodes of the cut meniscal horn edge to a single node on the tibial mesh for each meniscal horn (see Figure 3.9). Each meniscal horn used a spring stiffness of 350 N/mm [42]. This figure was divided by the number of springs attached to each node of the meniscal horn edges to obtain the individual spring stiffness.

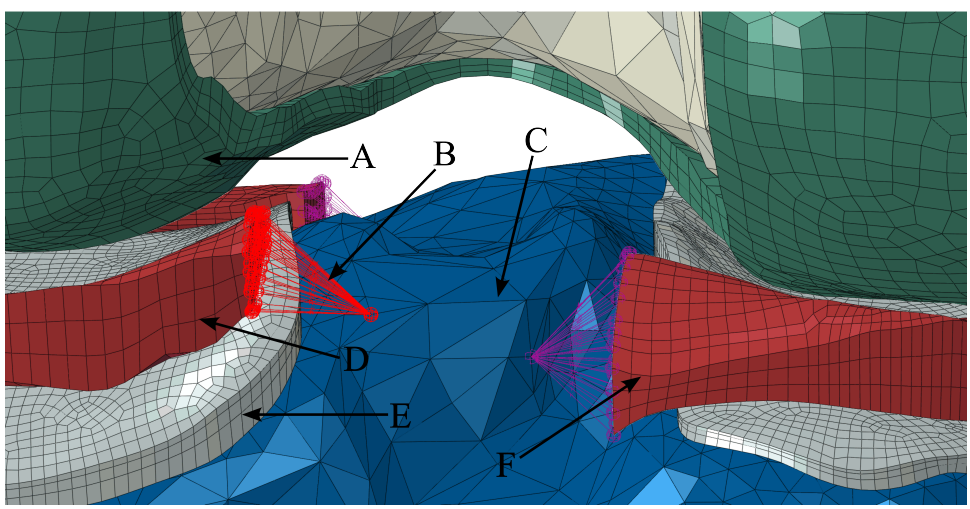

Figure 3.9: The edges of the menisci attached by spring elements to nodes on the tibia. **A**) The femoral cartilage **B**) The lateral posterior meniscus attachment **C**) The tibia **D**) The lateral posterior meniscal horn **E**) The lateral tibial cartilage **F**) The medial posterior meniscal horn.

Interactions

Femoral and tibial cartilage were attached to respective bones by a Tie condition. The contact interactions in the model were defined using the "Hard contact" surface-to-surface contact definition. These are seen in Figure 3.10. For the rigid bone models, a Rigid constraint was defined from a reference point in the femur and tibia respectively. For the deformable bone models, the constraint was defined as a Coupling from the reference points to the femoral and tibial surfaces respectively.

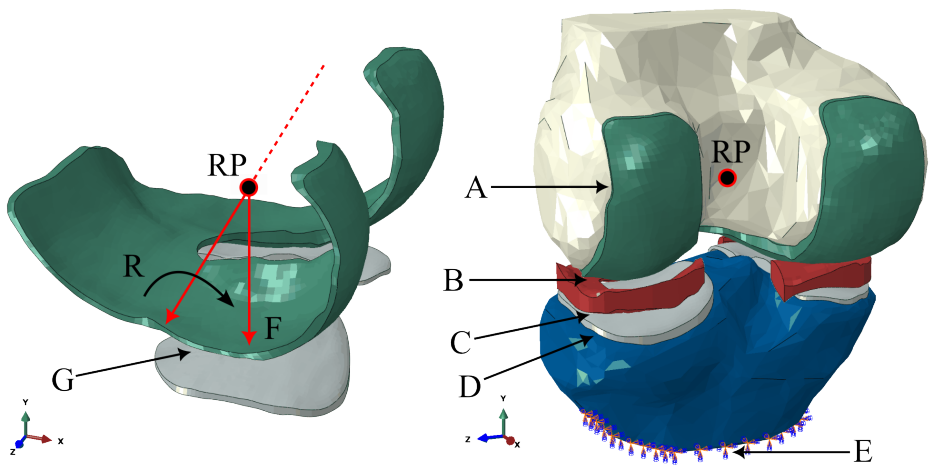

Figure 3.10: The interactions and boundary conditions applied to the knee models. **A**) Tie condition fixing the inner surface of the femoral cartilage (green) to the femur (white). **B**) Hard contact between femoral cartilage and menisci (red). **C**) Hard contact between menisci and tibial cartilage (grey). **D**) Tie condition fixing the inner surface of the tibial cartilage (grey) to the tibia (blue). **E**) Boundary condition restricting all degrees of freedom for the nodes of the distal surface of the tibia. **F**) Axial force defined from the reference point **RP** applied to the femur and femoral cartilage. **G**) Hard contact between femoral and tibial cartilage. **R**) Flexion-extension defined from the reference point **RP** applied to the femur and femoral cartilage.

Boundary conditions

A single reference point (denoted RP in Figure 3.10) was defined centrally in the femur, approximately at the midpoint between the condyles.

The forces, displacements, and rotations of the subject-specific weight and gait data applied to the knee were defined from this point (see Figure 3.10) in three steps in Abaqus (see Table 3.2).

Table 3.2: The three steps used in the Abaqus simulation.

Step	Boundary condition	Description
Step 0	Initial contact	2.5 mm axial displacement of the femur until femoral cartilage is in contact with the tibial cartilage.
Step 1	Body weight	Axial knee contact force equivalent to body weight on one knee while standing.
Step 2	Gait	Subject specific axial knee contact force and flexion-extension. The femur is allowed unrestricted rotation in the frontal plane to improve contact with the tibial cartilage.

In the rigid bone models, all degrees of freedom in the tibia were set to zero. For the deformable bone models, only the nodes of the distal surface of the tibia were fixed, restricting all degrees of freedom.

3.3.3 Post-processing

From the completed simulations, contour plots were made of the femoral cartilage, tibial cartilage and menisci, showing Von Mises stress, contact pressure and maximum principal strain at the first force peak, midstance and second force peak of the stance phase (see Figure 3.2). For the heterogeneous and SBC models, additional contour plots were made of the tibial bone showing minimum principal stress and strain distribution. In addition to this, for all models, a Matlab script was written to plot Von Mises stress, contact pressure and maximum principal strain in all surface nodes of the tibial cartilage exceeding a threshold of 0.1 MPa in contact pressure, as was implemented by Halonen et al. [8]. The average of all nodes passing the threshold as well as the node with the highest value was plotted for each time increment of the gait step. The average Von Mises stress and maximum principal strain for all nodes in the SBC was also plotted for each time increment of the gait step.

The PC used to run the simulations was equipped with an Intel Core i5-4590 CPU and 32 GB of RAM.

3.4 Summary of the finite element models

In total, four FE models of the knee were created and nine simulations were run for the three body weights.

- **Model 1: Rigid homogeneous bones**
  First simulated for Step 0 (see Table 3.2 for step configuration) and Step 1 at baseline weight for a comparison with Model 2. Subsequently simulated for Step 2 at baseline, 16 weeks and 68 weeks.
- **Model 2: Deformable homogeneous bones**
  Simulated for Step 0 and Step 1 at baseline weight for a comparison with Model 1.
- **Model 3: Heterogeneous tibia**
  Simulated for all steps at baseline and 16 weeks.
- **Model 4: Heterogeneous tibia with SBC**
  Simulated for all steps at baseline and 16 weeks.

The results of models 1 and 2 were compared to determine if there were differences in the resulting Von Mises stress, contact pressure, and maximum principal strain in the tibial cartilage of the models, and thereby conclude if modeling bone as rigid would be a suitable measure to decrease the computation time of the model. The more suitable of the two models would then be simulated for the three different sets of body weight and subject specific gait data to meet the main objective of the thesis.

To meet the secondary objectives of the thesis, models 3 and 4 were analyzed to determine if the heterogeneous structure or the SBC would have any impact on the Von Mises stress, contact pressure, or maximum principal strain in the tibial cartilage.

Chapter 4

Results

4.1 Comparing the rigid and deformable bone models

To understand the importance of assuming bone to be either rigid or deformable when modeling bone as an isotropic, homogeneous material, a comparison was made of the resulting Von Mises stress, contact pressure and maximum principal strain in the tibial cartilage of the rigid bone model and the homogeneous, cortical, deformable bone model. The simulations showed that these parameters varied by less than 1 % between the models at peak load. The computation time of the rigid bone model was 73 % less than that of the deformable homogeneous bone model. The rigid bone model was therefore chosen to simulate the effects of weight loss on cartilage in this thesis.

4.2 The effect of weight loss using rigid bone

To estimate the effect of weight loss on cartilage biomechanics, the results of the gait simulation using rigid bone were analyzed for Von Mises stress, contact pressure, and maximum principal strain using contour plots and nodal values throughout the gait step. Contour plots of these parameters were made for the first force peak, midstance, and the second force peak of the stance phase for the three different body weights of the subject: 85 kg at baseline, 74 kg at 16 weeks, and 72 kg at 68 weeks.

4.2.1 Von Mises stress

Von Mises stress in the cartilage and menisci decreased as the weight decreased from 85 kg at baseline to 74 kg at 16 weeks, particularly in concentrated areas where the stress exceeds 5 MPa (see Figures 4.1-4.3). The peak average Von Mises stress for nodes passing the contact pressure threshold of 0.1 MPa in the lateral tibial cartilage decreased by 6.9 % between baseline and 16 weeks. The peak average Von Mises stress decreased by 1.6 % between 16 and 68 weeks (see Figure 4.4). The maximum nodal Von Mises stress can be found in the appendix (see Figure 7.1)

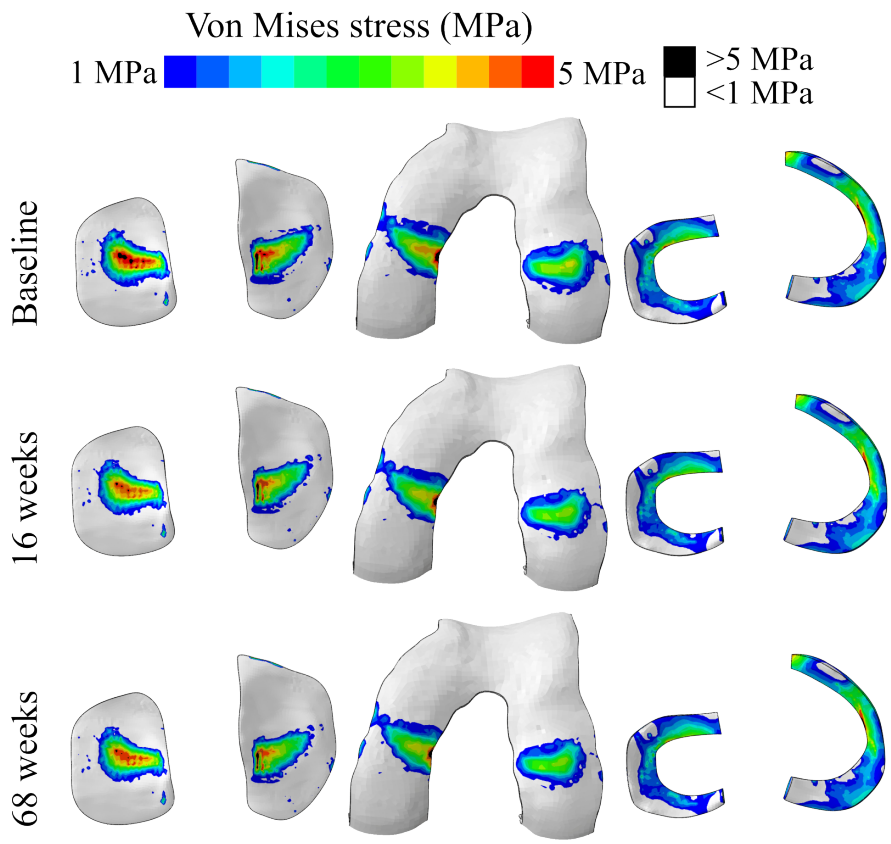

Figure 4.1: Von Mises stress at the first force peak (see Figure 3.2) of the stance phase for the tibial cartilage, femoral cartilage and menisci.

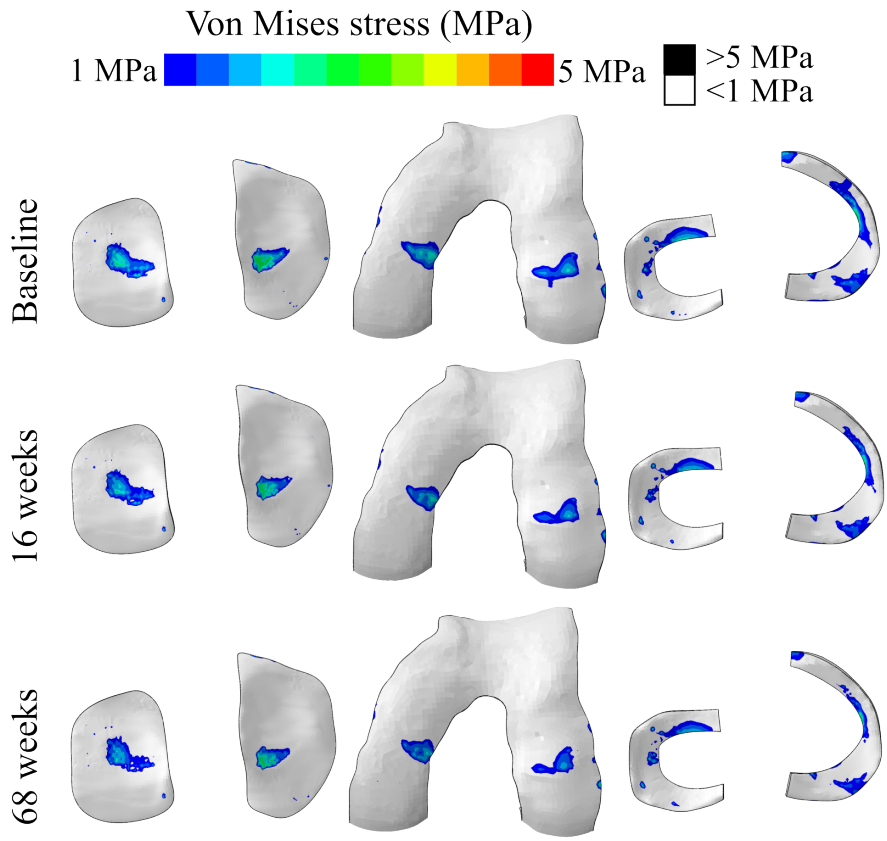

Figure 4.2: Von Mises stress at midstance (see Figure 3.2) of the stance phase for the tibial cartilage, femoral cartilage and menisci.

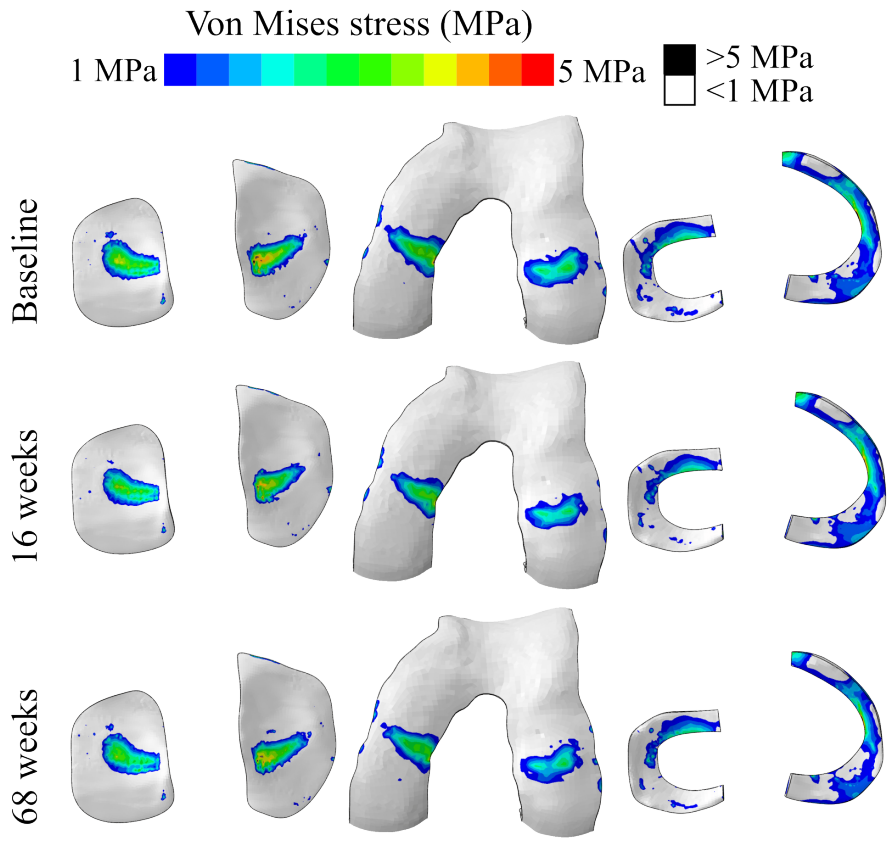

Figure 4.3: Von Mises stress at the second force peak (see Figure 3.2) of the stance phase for the tibial cartilage, femoral cartilage and menisci.

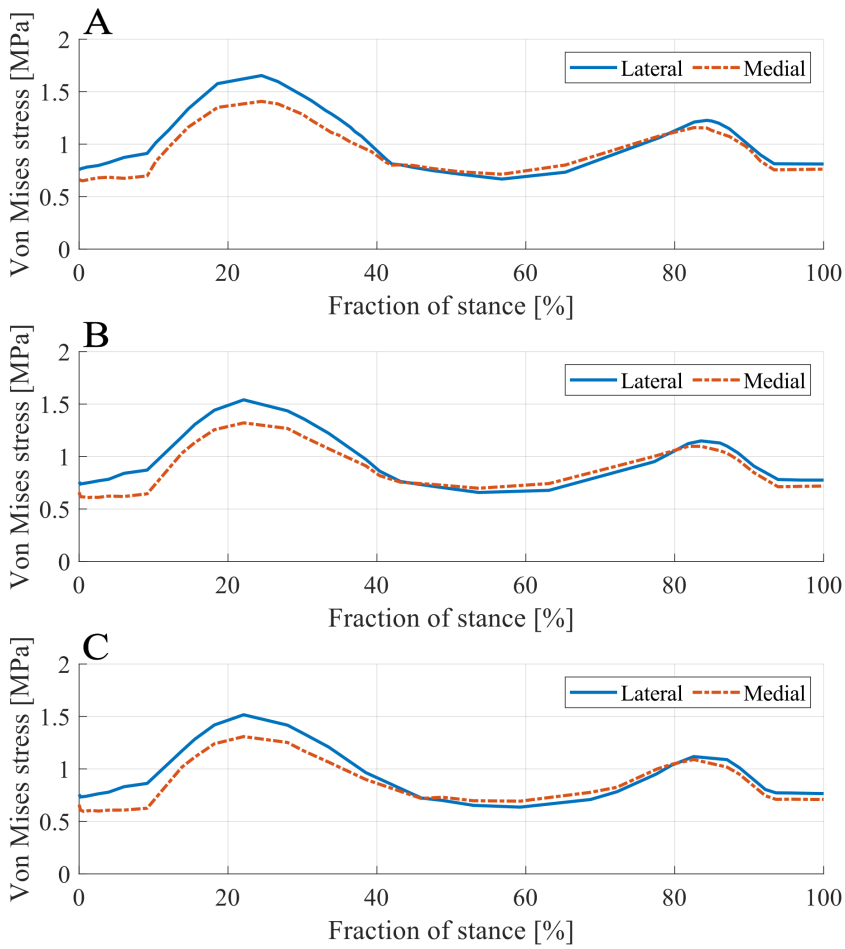

Figure 4.4: The average Von Mises stress of all nodes in the tibial cartilage of the rigid model passing the threshold of 0.1 MPa in contact pressure at each time increment of the gait step for **A**) baseline **B**) 16 weeks **C**) 68 weeks

4.2.2 Contact pressure

Contact pressure decreased by the largest margin between baseline and 16 weeks, with peak averaged contact pressure for the nodes passing the contact threshold decreasing by 6.2 % (see Figures 4.5-4.8). The contact pressure in the menisci was small compared to the tibial and femoral cartilage. The difference in peak contact pressure between 16 and 68 weeks was 1.9 %. Compared to the results for Von Mises stress (Figure 4.4), the difference in contact pressure between the medial and lateral tibial cartilage is smaller throughout the gait cycle. The maximum nodal contact pressure can be found in the appendix (see Figure 7.2).

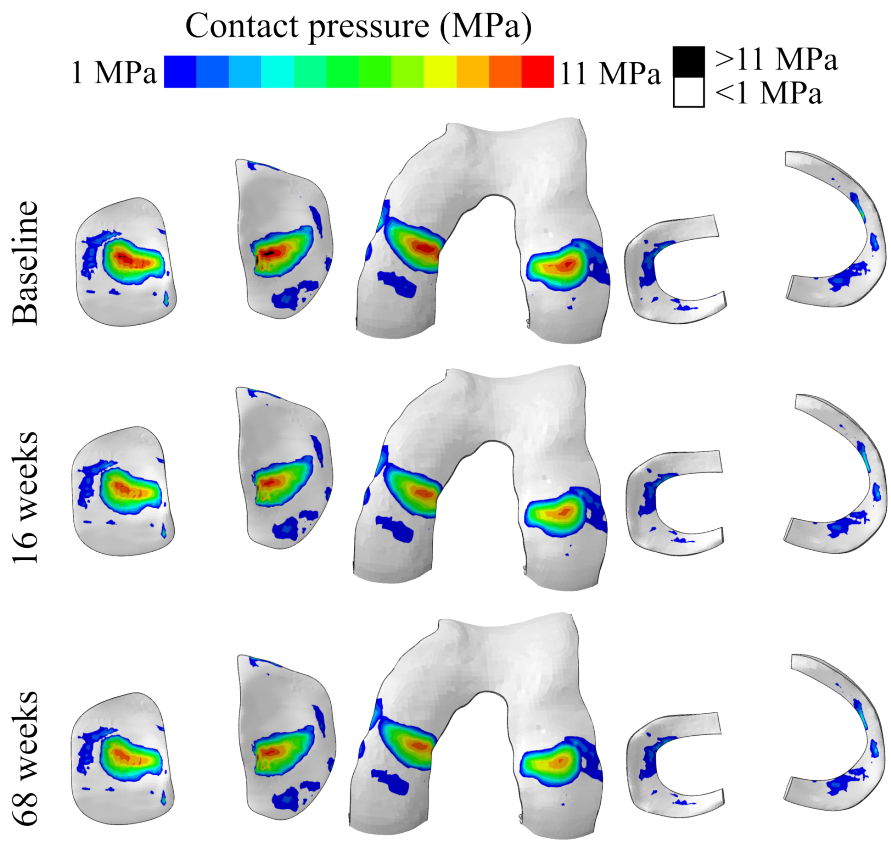

Figure 4.5: Contact pressure at the first force peak (see Figure 3.2) of the stance phase for the tibial cartilage, femoral cartilage and menisci.

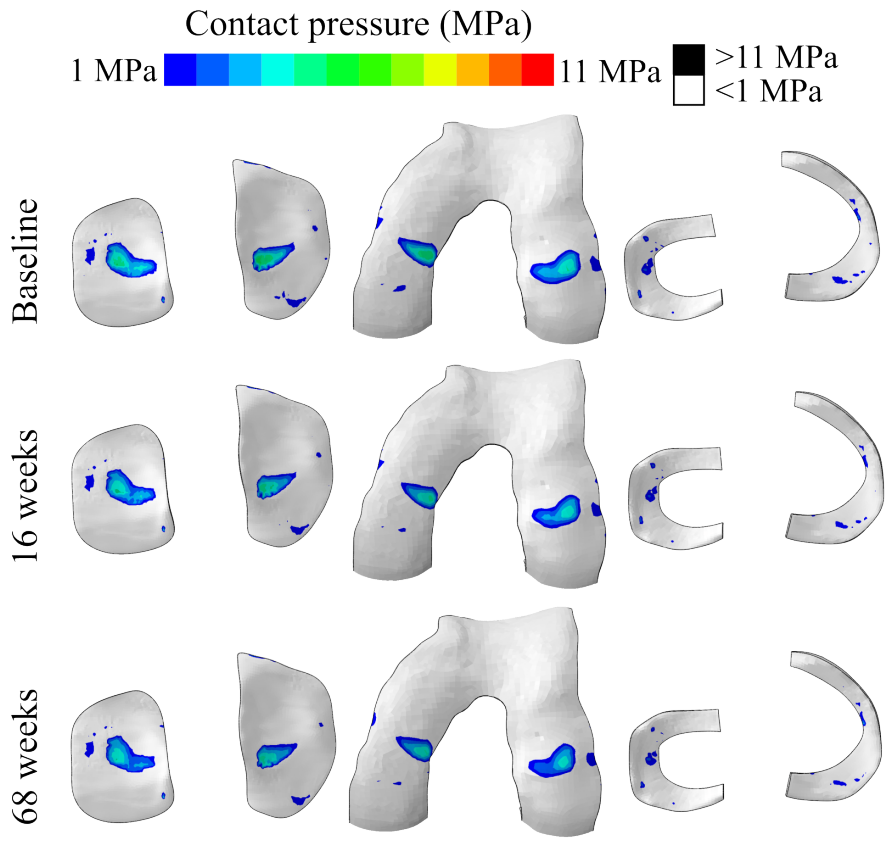

Figure 4.6: Contact pressure at midstance (see Figure 3.2) of the stance phase for the tibial cartilage, femoral cartilage and menisci.

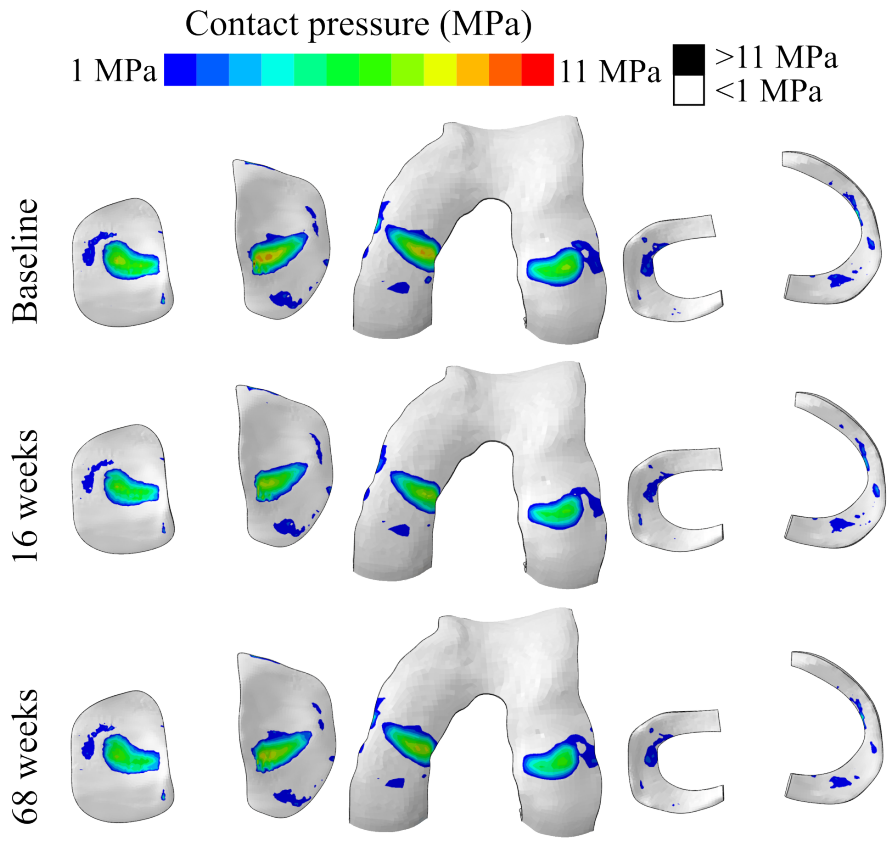

Figure 4.7: Contact pressure at the second force peak (see Figure 3.2) of the stance phase for the tibial cartilage, femoral cartilage and menisci.

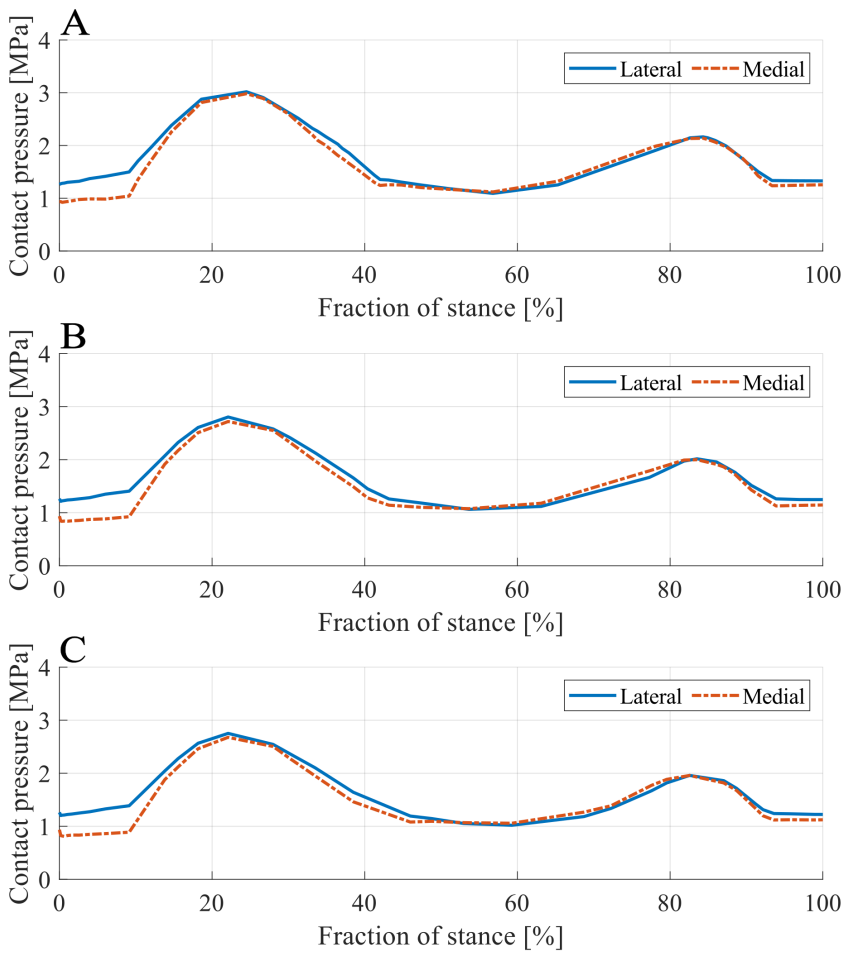

Figure 4.8: The average contact pressure of all nodes in the tibial cartilage of the rigid model passing the threshold of 0.1 MPa in contact pressure at each time increment of the gait step for **A**) baseline **B**) 16 weeks **C**) 68 weeks

4.2.3 Maximum principal strain

Like Von Mises stress and contact pressure, the maximum principal strain also decreased by the largest margin between baseline and 16 weeks (see Figures 4.9-4.11). Strain in the menisci is very high compared to the tibial and femoral cartilage. The peak strain in the lateral tibial cartilage decreased by 6.5 % between baseline and 16 weeks, while it decreased by 1.4 % between 16 and 68 weeks (Figure 4.12). See the appendix for the highest nodal maximum principal strain (Figure 7.3).

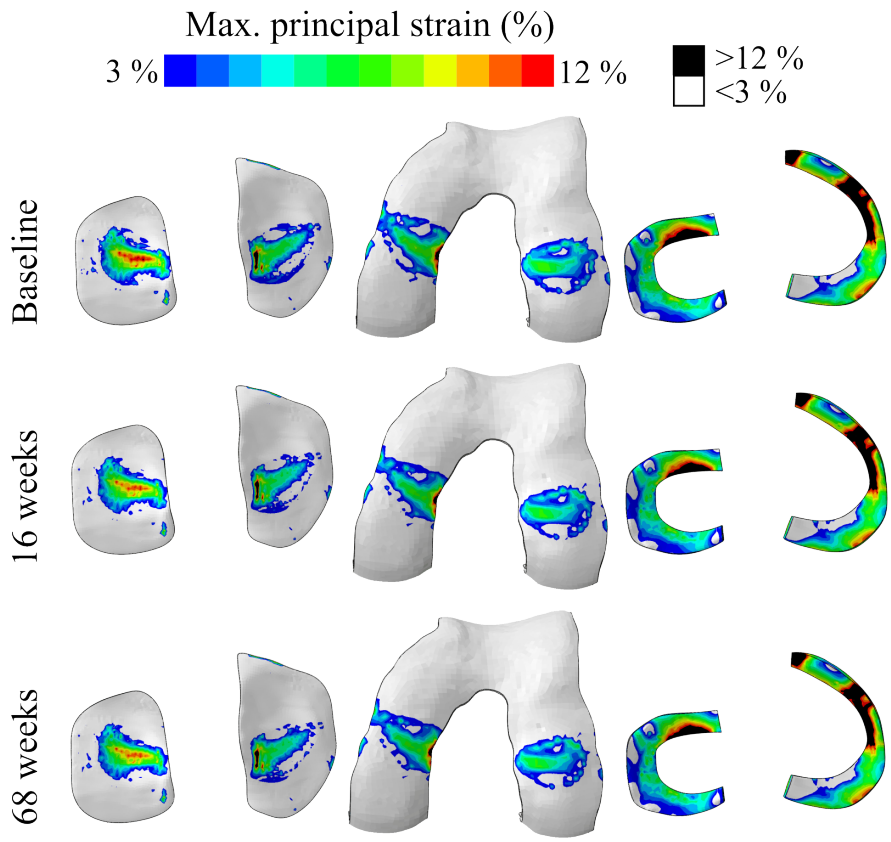

Figure 4.9: Maximum principal strain at the first force peak (see Figure 3.2) of the stance phase for the tibial cartilage, femoral cartilage and menisci.

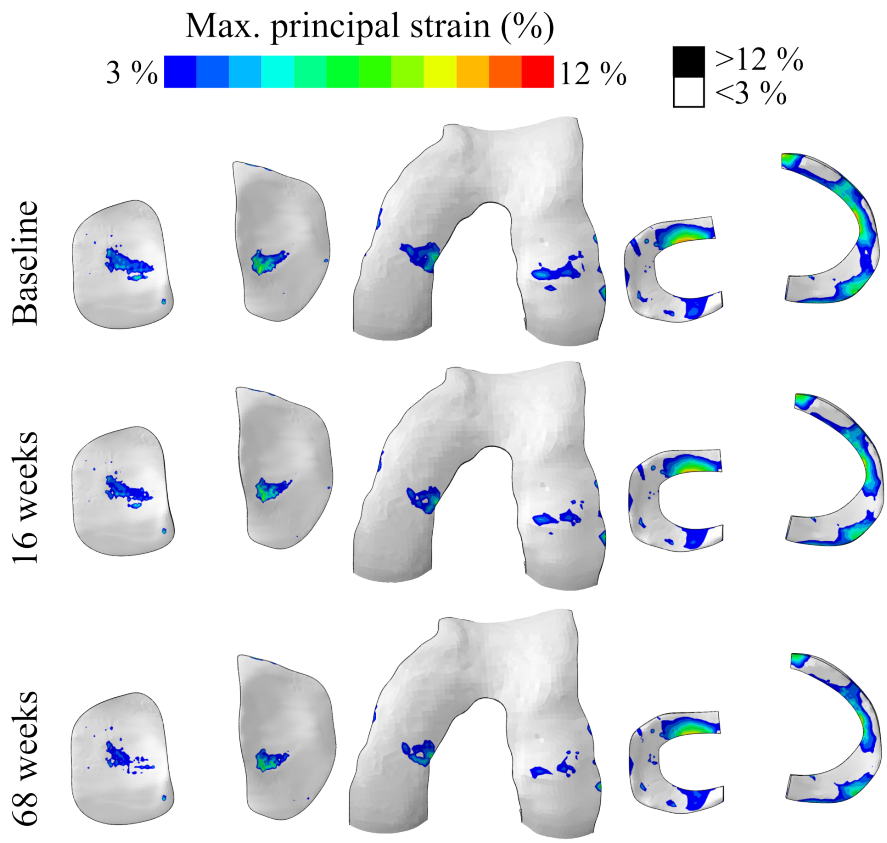

Figure 4.10: Maximum principal strain at midstance (see Figure 3.2) of the stance phase for the tibial cartilage, femoral cartilage and menisci.

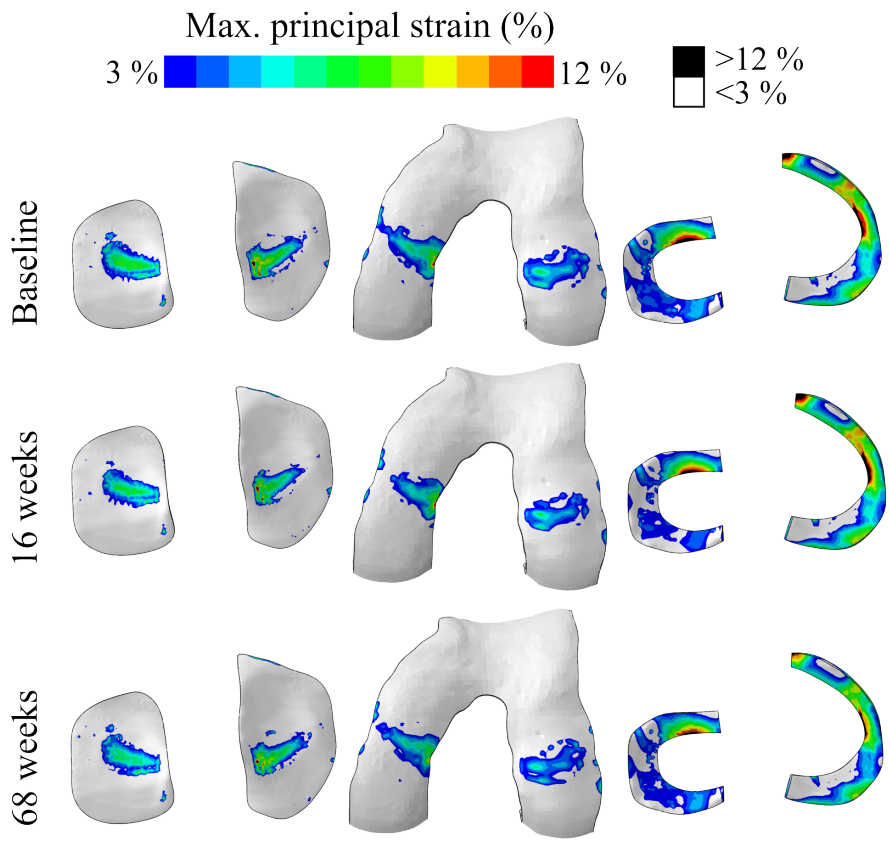

Figure 4.11: Maximum principal strain at the second force peak (see Figure 3.2) of the stance phase for the tibial cartilage, femoral cartilage and menisci.

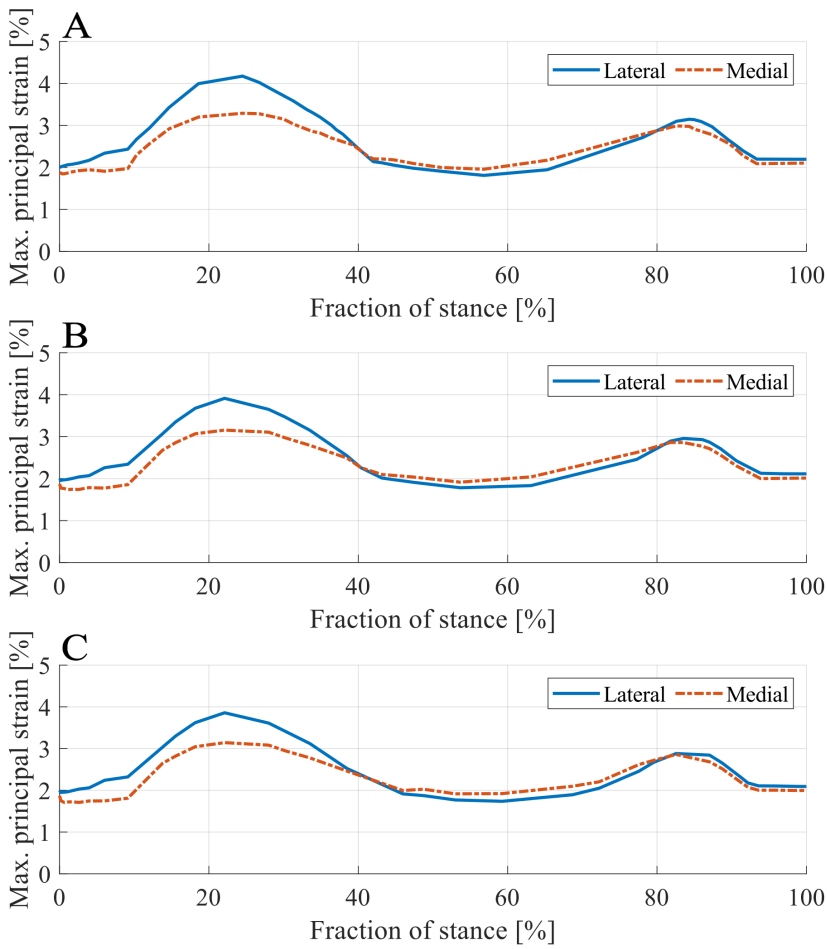

Figure 4.12: The maximum principal strain of all nodes in the tibial cartilage of the rigid model passing the threshold of 0.1 MPa in contact pressure at each time increment of the gait step for **A**) baseline **B**) 16 weeks **C**) 68 weeks

4.3 The heterogeneous bone model

In the model using a heterogeneous tibia, the peak averaged contact pressure, Von Mises stress, and maximum principal strain of all nodes in the tibial cartilage passing the contact pressure threshold of 0.1 MPa was 1.8 %, 10.7 %, and 14.8 % less respectively than the rigid tibia model at baseline weight (85 kg) (see Figure 4.13). Maximum nodal values can be found in the appendix (Figure 7.4).

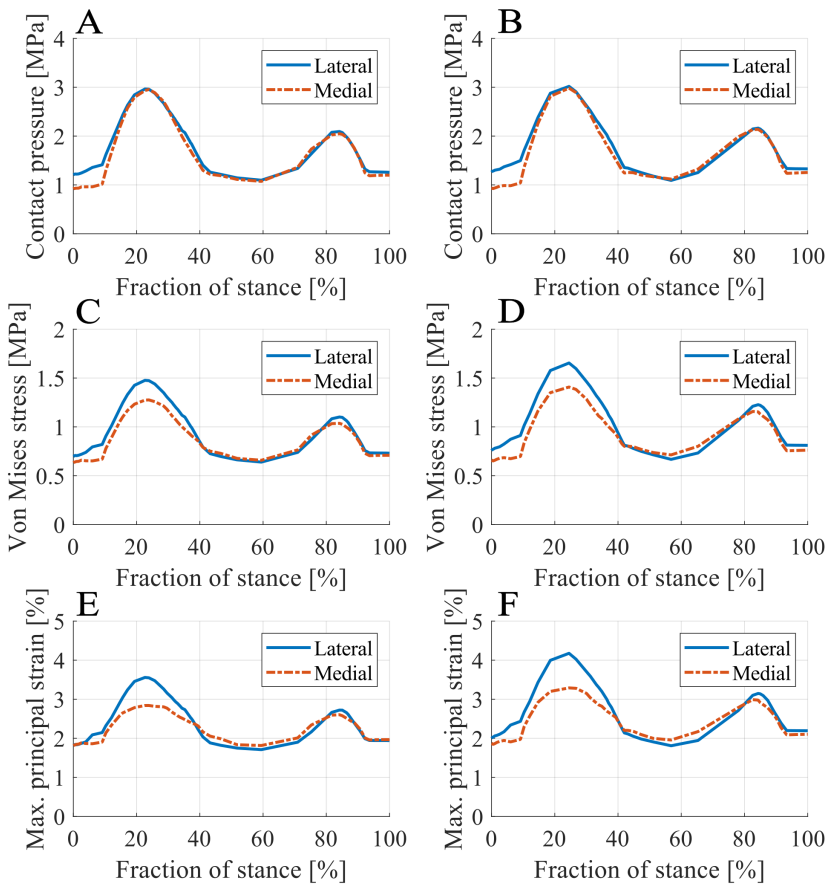

Figure 4.13: For all nodes passing the contact pressure threshold of 0.1 MPa in the tibial cartilage at baseline weight, the averaged contact pressure for **A**) the heterogeneous model **B**) the rigid model, the averaged Von Mises stress for **C**) the heterogeneous model **D**) the rigid model, the averaged maximum principal strain for **E**) the heterogeneous model **F**) the rigid model.

4.4 Comparing the heterogeneous and cyst models

To examine the effect of the subchondral bone cyst on cartilage and bone, the results of the SBC model were compared to the heterogeneous model at baseline weight (85 kg) and 16 weeks (74 kg). The difference in peak averaged contact pressure, Von Mises stress, and maximum principal strain of the nodes passing the threshold in the lateral tibial cartilage was less than 1 % between the heterogeneous and SBC models at baseline weight (see Figure 4.14). The peak average contact pressure, Von Mises stress, and maximum principal strain in the medial cartilage were 2.7 %, 2.5 %, and 1.9 % lower respectively in the medial cartilage of the SBC model at baseline weight.

Between baseline weight and at 16 weeks, peak averaged contact pressure, Von Mises stress, and maximum principal strain decreased by 9.5 %, 8.8 %, and 7.7 % respectively in the lateral cartilage. The same parameters decreased by 7.7 %, 4.5 %, and 2.3 % respectively from baseline to 16 weeks in the medial cartilage. Inclusion of the SBC led to an increase in the minimum principal stress and strain in the bone in proximity to the SBC when compared to the heterogeneous tibia (see Figure 4.16). Maximum principal stress and strain in the bone changed by only a small margin due to the SBC. Both models display higher strain in the medial side of the tibial bone than the lateral. At peak load of the gait step, the average Von Mises stress and maximum principal strain of all nodes in the SBC decreased by 13.7 percent and 12.2 percent respectively between baseline and 16 weeks (Figure 4.17). The maximum nodal values can be seen in the appendix (Figure 7.5).

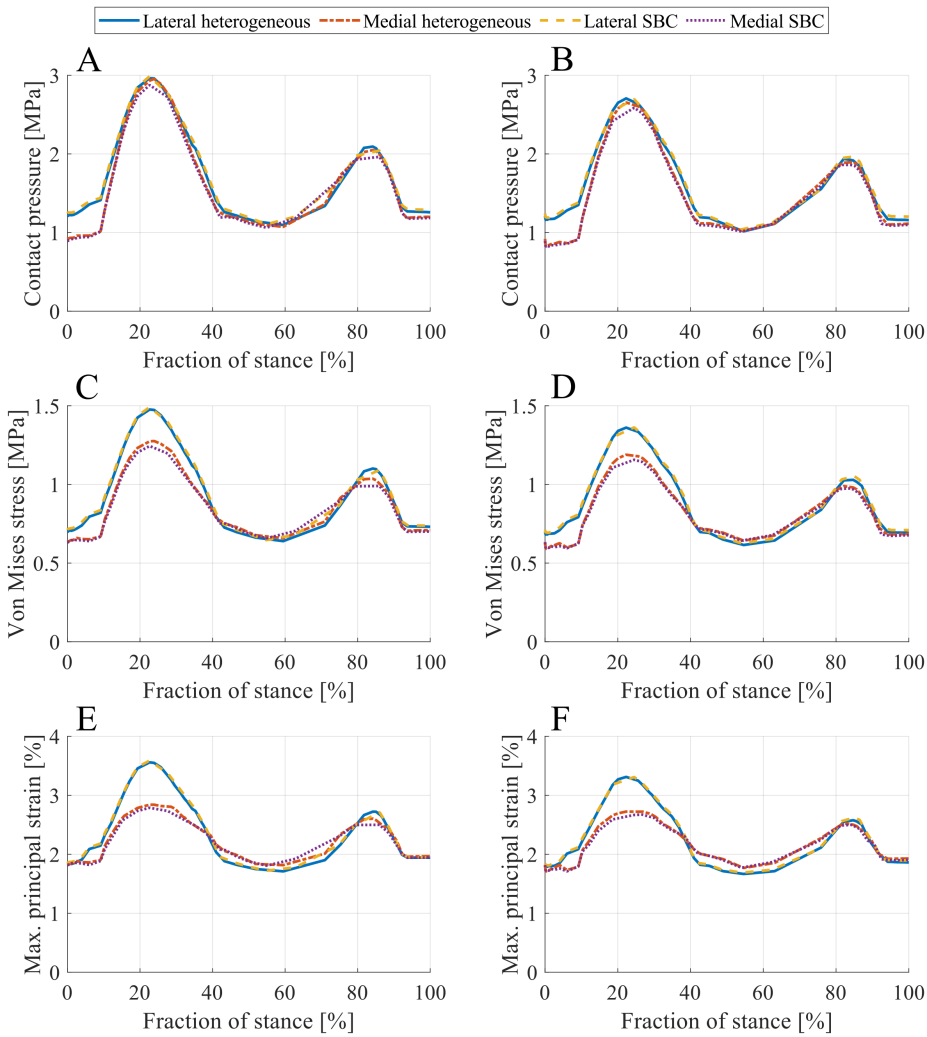

Figure 4.14: For all nodes passing the contact pressure threshold of 0.1 MPa in the tibial cartilage of the heterogeneous and SBC models, contact pressure at **A**) baseline **B**) 16 weeks, Von Mises stress at **C**) baseline **D**) 16 weeks, maximum principal strain at **E**) baseline **F**) 16 weeks.

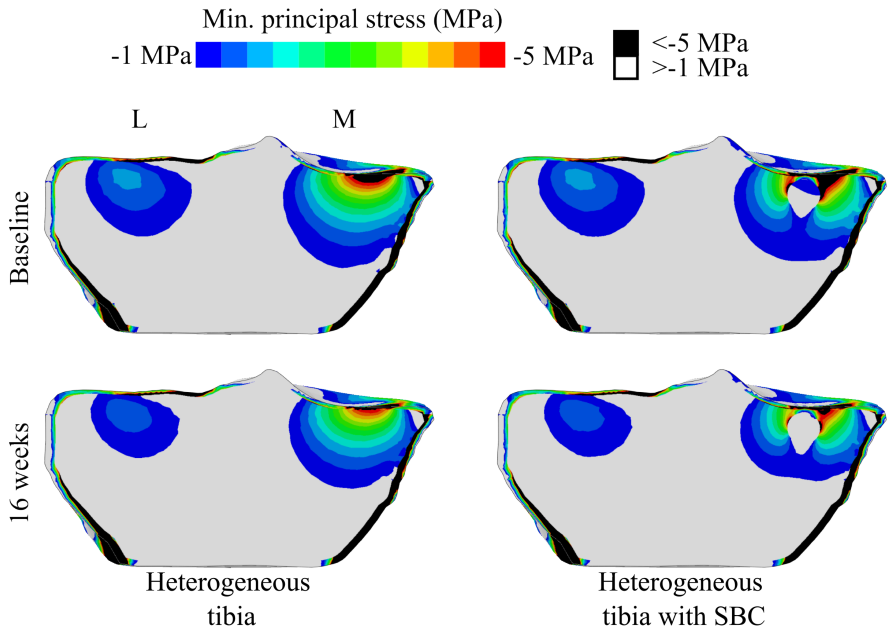

Figure 4.15: Minimum principal stress in the tibia for the heterogeneous and SBC bone models at the first force peak (see Figure 3.2).

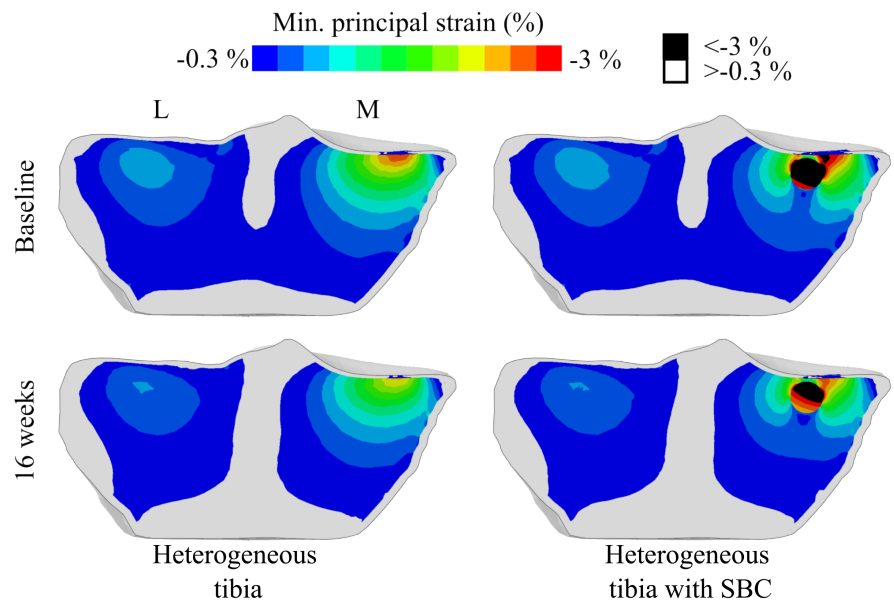

Figure 4.16: Minimum principal strain in the tibia for the heterogeneous and SBC bone models at the first force peak (see Figure 3.2).

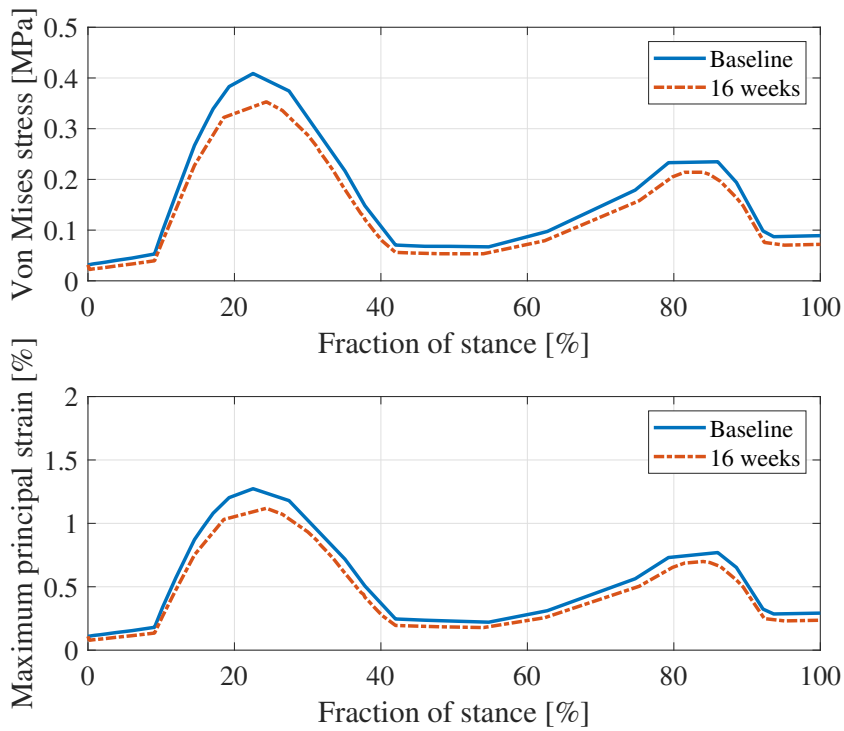

Figure 4.17: Averaged Von Mises stress and maximum principal strain for all nodes in the subchondral bone cyst over the course of the gait step.

Chapter 5

Discussion

This thesis aimed to use a subject-specific finite element knee model to investigate the effects of weight loss on cartilage biomechanics. Based on MRI data of one subject participating in the CAROT trial [13], a 3D volume of a left knee joint was segmented, meshed, and simulated for subject-specific gait and three loading scenarios based on the altering physical weight of the patient using four different FE models in Abaqus. The results of the simulations showed that weight loss led to lower contact pressure, Von Mises stress, and maximum principal strain in the cartilage.

5.1 The rigid bone model

When modeling bone as a homogeneous material using a cortical bone material model, the results of the simulations showed that treating the geometry as rigid is an assumption that saves computation time without major loss in accuracy in the predicted cartilage mechanics.

When the weight in the gait simulations decreased by 13 % between baseline and 16 weeks, contact pressure, stress, and strain at peak load in the tibial cartilage decreased by 6.2, 6.9, and 6.5 % respectively. This suggests that the relationship between weight and mechanical load on the tibial cartilage is not linear.

A study that implemented a fully deformable linear elastic knee model reported a peak of approximately 2 MPa of Von Mises stress in the femoral cartilage when applying 800 N of axial load in full extension of the knee [43]. In comparison, the axial load at the second force peak of the gait simulation in this thesis was 1227 N, and the peak Von

Mises stress was approximately 4 MPa in the femoral and tibial cartilage (see Figure 4.3). The stresses are however concentrated in different areas of the femoral and tibial cartilage, while the stress concentrations in the menisci are somewhat similar.

The high strain in proximity to the posterior medial meniscal horn may indicate that this meniscal horn was modeled or attached incorrectly. Similarly, the anterior sections of the menisci show lower Von Mises stress and maximum principal strain than the posterior sections. This contradicts some theories and observations that the posterior sections of the menisci sustain higher loads [44]. The contact pressure, Von Mises stress, and maximum principal strain in the inner surfaces of the menisci do however indicate that these areas are where the menisci provide the most support to the cartilage. Modeling the menisci as isotropic may have contributed to the high strain. An alternative could have been to model the menisci as transversely isotropic [8]. Dispersing the spring attachments over a greater number of nodes may also have been an approach to more accurately model the meniscal attachments.

A study investigating the effects of knee meniscal implants on cartilage contact pressure using FE modeling reported values of contact pressure similar to those in this thesis [45]. Using a transversely isotropic, nearly incompressible Neo-Hookean hyperelastic material model for the menisci, the study reported peak contact pressures of 7.5 MPa in the tibial and femoral cartilage for an axial load of 1200 N in full extension of the knee. The 1227 N of axial load at the second force peak of the gait simulation resulted in maximum contact pressures of approximately 9 MPa in the femoral and tibial cartilage (see Figure 4.7), a 20 % difference in contact pressure for a similar load.

Of note in the model is that the average nodal stresses and strains are higher in the lateral cartilage. This contradicts the fact that the medial compartment of the tibiofemoral joint generally sustains higher loads [46]. A possible reason for this could be that the free varus-valgus rotation of the femur in the gait step of the simulations does not fully account for the in-vivo loading conditions in the joint. The maximum nodal stresses and strains in the tibial cartilage are however higher in the medial compartment.

Clinical follow-up in the CAROT trial [32] of the subject investigated in this thesis examined changes in the cartilage from baseline to 68 weeks. The cartilage was given a blind score by a radiologist using the Boston-Leeds Osteoarthritis Knee Score (BLOKS) method [47]. This

method gives the cartilage a score of 0, 1, 2, or 3 depending on the severity of OA, 0 being no evidence of OA and 3 being severe OA. The examination revealed that the subject had BLOKS grade 1 in the lateral tibial cartilage at all time points. The medial tibial cartilage had BLOKS grade 1 at baseline and 16 weeks, decreasing to BLOKS grade 0 at 68 weeks [32]. The decrease in Von Mises stress, contact pressure, or maximum principal strain between baseline and 68 weeks could therefore be indicative of a threshold where the joint may possibly recover. However, it may also be indicative of the low sensitivity of the BLOKS score.

The clinical follow-up also examined joint pain experienced by the subject using the visual analog scale (VAS). This grading system rates pain from 0 as no pain, to 100 as severe pain. The subject reported 10 at baseline and 2 at 16 as well as 68 weeks. This could also be indicative of mechanical thresholds for pain related to OA.

5.2 The heterogeneous tibia model

Using a deformable, heterogeneous tibia model in the gait simulation led to lower contact pressure, Von Mises stress, and maximum principal strain in the tibial cartilage. This was perhaps an expected result, as the bone was allowed to deform. The load applied in the simulation was generally transmitted only to the subchondral and cortical bone, as the minimum principal stress of the trabecular bone was comparatively low. In contrast to the higher average stress, strain, and contact pressure in the tibial cartilage, the minimum principal stress in the medial compartment is higher. A possible reason could be thinner subchondral bone in the medial compartment of the model. Modeling the femur as deformable and heterogeneous as well could have had an impact on the loads sustained by the tibial cartilage, but remains to be investigated.

5.3 The subchondral bone cyst model

The addition of a subchondral bone cyst had an impact of less than 1 % on the Von Mises stress, maximum principal strain, and contact pressure in the tibial cartilage when compared to the heterogeneous tibia without a SBC. Despite the proximity of the cyst to the joint line, the mechanical effect on the surface nodes of the tibial cartilage

was small. The nodal average calculation in Figure 4.14 did however only take into account surface nodes on the tibial cartilage. Expanding the calculation to include the average Von Mises stress and maximum principal strain of all nodes in the tibial cartilage may have produced another picture of the stresses and strains, as the SBC could affect the tibial cartilage closer to the subchondral bone. The effects were however seen in the minimum principal stress and strain in the trabecular and subchondral bone, similar to what was observed by Anwar et al. [41]. The increase in strain in the trabecular bone close to the cyst at baseline weight (Figure 4.16) could indicate a volume of bone under high risk of fracture, as the yield strain of trabecular bone is in the range of 2-4 % [14]. To more thoroughly assess the effects on cartilage and bone, several SBCs could have been included, as well as SBCs in the lateral side to rule out the possibility of variations in the subchondral bone thickness of the two compartments.

Though the trial participant that was examined in this thesis did not have a subchondral bone cyst, the decrease in Von Mises stress and maximum principal strain in the SBC of 13.7 % and 12.2 % respectively, as well as the reduction of minimum principal stress and strain in the bone in the simulation could also be indicative of mechanical thresholds for pain reduction in cases of OA where SBC's are present.

5.4 Limitations

In this thesis, segmentation of the knee joint was performed manually on MRI data. This proved difficult due to the limited contrast and resolution of the image stack. Combined with large slice thickness, this led to low detail in some features of the segmentation, particularly of the bone and menisci.

Furthermore, the boundary conditions of the simulations applied only axial force and flexion-extension in the knee. Factoring in the subject-specific varus-valgus and internal-external rotation of the knee in the input data would have yielded a simulation closer to in-vivo loading conditions, despite those rotations being small in comparison to flexion-extension. Varus-valgus rotation was unrestricted in the gait step of the simulation, but how it compared to the true varus-valgus rotation of the subject or generic gait data was not investigated. Addition of the collateral and cruciate ligaments to the model, either in segmented form or represented by springs, would also have contributed

to boundary conditions closer to in-vivo loading conditions, and would have naturally restricted varus-valgus and internal-external rotation. The models that were explored in this thesis restricted all other degrees of freedom to zero, limiting the similarity of the simulations to the in-vivo knee kinematics of gait.

The models simulated in this thesis also implemented a Neo-Hookean hyperelastic material model for cartilage. While this material model can account for more of the mechanical behavior of cartilage than for example a linear elastic material model, other alternatives such as poroelastic and fibril-reinforced models can be superior when modeling cartilage [12], although also being more computationally demanding.

The muscle tissue of the knee was not segmented and therefore not included in the 3D model. The mechanical effect of the muscles were however taken into account in the gait data acquired in the CAROT study through motion analysis and use of an OpenSIM-model. Therefore the principal effect of the muscles on the mechanics of the knee model is accounted for but not explicitly included in the FE mesh.

In this thesis, no convergence analysis of the mesh was performed. The approximate element size for the cartilage and menisci in the models were however derived from another study [2]. As for the tetrahedral bone mesh used in the heterogeneous and SBC models, it is not known if a finer mesh would have resulted in different minimum principal stress and strain values. Using quadratic hexahedral elements (C3D20) for the cartilage and menisci could have produced more accurate contact interaction between the soft tissues, but would also have increased the computation time.

5.5 Future perspective

The work of this thesis showed that stresses, strains, and contact pressure in knee cartilage change as body weight decreases. With more time, several improvements to the models could have been implemented. Ligament representations could be added for more anatomically accurate restriction of the degrees of freedom of the knee joint. A model using a deformable heterogeneous femur as well as tibia would be of interest to simulate to observe any possible effects on the cartilage. The nodal analysis of stresses, strains, and contact pressure in the tibial cartilage could be extended to the femoral cartilage as well for a more thorough analysis of all cartilage structures of the knee.

In this thesis, all FE models used gait data measured at baseline weight (85 kg). The results of this thesis would have been of interest to compare to models based on gait data from 16 weeks (74 kg) and 68 weeks (72 kg), to see if changes in gait pattern affect the cartilage along with the decrease in weight.

With further validation of the models simulated in this thesis, improvements in computational power, or suitable simplification of the models, assessing the risk OA on a subject-specific basis using numerical modeling could in the future become a powerful tool in healthcare. An effective simulation of the biomechanics of knee cartilage could provide more options for preventative treatment of a disease that is difficult to treat after symptoms begin to manifest.

5.6 Ethical aspects

To create the knee FE models in this thesis, MRI images of the left knee from a participant in the CAROT study were used. Participation in the study was voluntary, the data was rendered anonymous, and the participants gave written informed consent approved by the ethics committee of the Capital Region of Denmark [H-B-2007-088] [13].

Numerical modeling of the knee joint as done in this thesis has implications for the treatment of OA. If the biomechanical impact of weight loss on knee cartilage using FE analysis can be quantified and validated, the method could be applied in the clinic to determine the best possible way to treat OA. From a beneficence ethics perspective, this would be very positive as it presents a new alternative of determining treatment of a complex disease. The method could reduce the cost of OA to healthcare systems by providing improved preventative treatment that avoids the scenario where patients must undergo expensive procedures such as TKR.

Using numerical modeling to assess the risk subject-specific of OA is however a technology intense procedure. A future clinical application would require access to MRI scanners, computational resources, motion analysis systems, and likely a significant amount of labor to produce and simulate the model. Using this method would be very expensive and likely only available in developed countries with access to advanced healthcare. From the point of view of justice ethics, this would be negative as the method would likely not be available to the majority of the global population. Patients with magnetic implants would also

be excluded from the procedure. Ways of automating the creation of numerical models of the knee joint and reducing the time it takes is an ongoing field of research [9] but is as yet a labor-intensive process.

In the future, development of the method may reach a point where an algorithm segments imaging data, runs a number of simulations and independently suggests the best course of treatment automatically. Clinical personnel would then be needed to analyse and confirm the suggested course of action to avoid shifting responsibility for the treatment to an algorithm.

Chapter 6

Conclusions

This thesis set out to estimate the effects of weight loss on cartilage biomechanics using a subject-specific 3D finite element knee model. Simulation of four different FE models for altering weight scenarios have led to the following conclusions.

- Weight loss simulated by FE analysis using subject-specific data lead to a reduction in contact pressure, Von Mises stress, and maximum principal strain in the tibial cartilage, femoral cartilage and menisci of the knee.
- Treating bone as rigid in the knee model provides a negligible loss of accuracy for cartilage mechanics compared to a homogeneous, cortical, and deformable bone model while substantially reducing computation time.
- Modeling the tibial bone as isotropic, heterogeneous, and deformable resulted in reduced Von Mises stress and maximum principal strain in the tibial cartilage when compared to the rigid model.
- Simulating a hypothetical scenario where the subject had a subchondral bone cyst in the medial compartment of an isotropic, heterogeneous, deformable tibia resulted in reduced contact pressure, Von Mises stress, and maximum principal strain when compared to the rigid model, but also a marginal decrease in these parameters when compared to a heterogeneous model without a cyst. The cyst did however contribute to altered minimum principal stress distribution and increased minimum principal strain in the trabecular bone in proximity to the cyst.

For future investigations, the knee FE models simulated in this thesis

can be expanded in terms of analysis, material models and addition of ligaments for a more in-depth analysis of the effect of weight loss in cartilage biomechanics. With further refinement of the FE models and workflow, numerical modeling of knee joint biomechanics could become a useful tool in the prediction and prevention of OA.

Bibliography

[1] Yuqing Zhang and Joanne M Jordan. Epidemiology of osteoarthritis. *Clinics in geriatric medicine*, 26(3):355–369, 2010.

[2] Mika E Mononen, Petri Tanska, Hanna Isaksson, and Rami K Korhonen. A novel method to simulate the progression of collagen degeneration of cartilage in the knee: data from the osteoarthritis initiative. *Scientific reports*, 6(1):1–14, 2016.

[3] Olesya Klets, Mika E Mononen, Mimmi K Liukkonen, Mika T Nevalainen, Miika T Nieminen, Simo Saarakkala, and Rami K Korhonen. Estimation of the effect of body weight on the development of osteoarthritis based on cumulative stresses in cartilage: data from the osteoarthritis initiative. *Annals of biomedical engineering*, 46(2):334–344, 2018.

[4] Aleksandra Turkiewicz. *Epidemiology of osteoarthritis in Sweden. Register and cohort studies on prevalence and mortality.* PhD thesis, Department of Clinical Sciences, Lund, 2016.

[5] MJ Nissi, J Rieppo, J Töyräs, MS Laasanen, I Kiviranta, MT Nieminen, and JS Jurvelin. Estimation of mechanical properties of articular cartilage with mri–dgemric, t2 and t1 imaging in different species with variable stages of maturation. *Osteoarthritis and Cartilage*, 15(10):1141–1148, 2007.

[6] WAM Brekelmans, HW Poort, and TJJH Slooff. A new method to analyse the mechanical behaviour of skeletal parts. *Acta Orthopaedica Scandinavica*, 43(5):301–317, 1972.

[7] Nicole M Grosland, Kiran H Shivanna, Vincent A Magnotta, Nicole A Kallemeyn, Nicole A DeVries, Srinivas C Tadepalli, and Curtis Lisle. IA-FEMesh: An open-source, interactive, multiblock

approach to anatomic finite element model development. *Computer methods and programs in biomedicine*, 94(1):96–107, 2009.

[8] KS Halonen, ME Mononen, JS Jurvelin, J Töyräs, and RK Korhonen. Importance of depth-wise distribution of collagen and proteoglycans in articular cartilage—a 3d finite element study of stresses and strains in human knee joint. *Journal of biomechanics*, 46(6):1184–1192, 2013.

[9] Clare K Fitzpatrick, Mark A Baldwin, and Paul J Rullkoetter. Computationally efficient finite element evaluation of natural patellofemoral mechanics. *Journal of biomechanical engineering*, 132(12), 2010.

[10] Hamid Naghibi Beidokhti, Dennis Janssen, Sebastiaan van de Groes, Javad Hazrati, Ton Van den Boogaard, and Nico Verdonschot. The influence of ligament modelling strategies on the predictive capability of finite element models of the human knee joint. *Journal of biomechanics*, 65:1–11, 2017.

[11] Gustavo A Orozco, Petri Tanska, Mika E Mononen, Kimmo S Halonen, and Rami K Korhonen. The effect of constitutive representations and structural constituents of ligaments on knee joint mechanics. *Scientific reports*, 8(1):1–15, 2018.

[12] Alexander Paz, Gustavo A Orozco, Rami K Korhonen, José J García, and Mika E Mononen. Expediting finite element analyses for subject-specific studies of knee osteoarthritis: A literature review. *Applied Sciences*, 11(23):11440, 2021.

[13] Robin Christensen, Marius Henriksen, Anthony R. Leeds, Henrik Gudbergsen, Pia Christensen, Tina J. Sørensen, Else M. Bartels, Birgit F. Riecke, Jens Aaboe, Rikke Frederiksen, Mikael Boesen, L. Stefan Lohmander, Arne Astrup, and Henning Bliddal. Effect of weight maintenance on symptoms of knee osteoarthritis in obese patients: A twelve-month randomized controlled trial. *Arthritis Care & Research*, 67(5):640–650, 2015.

[14] Margareta Nordin and Victor Frankel. *Basic Biomechanics of the Musculoskeletal System.* Wolters Kluwer Health/Lippincott Williams & Wilkins, Philadelphia, 2012.

[15] Joerg Eschweiler, Nils Horn, Bjoern Rath, Marcel Betsch, Alice Baroncini, Markus Tingart, and Filippo Migliorini. The biomechanics of cartilage—an overview. *Life*, 11(4):302, 2021.

[16] J.M. Mansour. *Biomechanics of cartilage*, pages 69–83. 2013.

[17] Susanne Grässel and Attila Aszódi. *Cartilage*, pages 2–5. Springer, 2016.

[18] Centers for Disease Control and Prevention. The Cost of Arthritis in US Adults, 2020. `https://www.cdc.gov/arthritis/data_statistics/cost.htm`. [Online; accessed 2022-06-04].

[19] Terence W O'Neill, Paul S McCabe, and John McBeth. Update on the epidemiology, risk factors and disease outcomes of osteoarthritis. *Best practice & research Clinical rheumatology*, 32(2):312–326, 2018.

[20] Somayeh Ebrahimkhani, Mohamed Hisham Jaward, Flavia M Cicuttini, Anuja Dharmaratne, Yuanyuan Wang, and Alba G Seco de Herrera. A review on segmentation of knee articular cartilage: from conventional methods towards deep learning. *Artificial intelligence in medicine*, 106:101851, 2020.

[21] Peter Cram, Xin Lu, Stephen L Kates, Jasvinder A Singh, Yue Li, and Brian R Wolf. Total knee arthroplasty volume, utilization, and outcomes among medicare beneficiaries, 1991-2010. *Jama*, 308(12):1227–1236, 2012.

[22] EL Radin, DB Burr, B Caterson, D Fyhrie, TD Brown, and R Boyd. Mechanical determinants of osteoarthrosis. In *Seminars in arthritis and rheumatism*, volume 21, pages 12–21. Elsevier, 1991.

[23] Vivek Pai and Henry Knipe. Kellgren and Lawrence system for classification of osteoarthritis, 2021. `https://doi.org/10.53347/rID-27111`. [Online; accessed 2022-06-04].

[24] J Jones and Y Baba. T1 weighted image, 2021. `https://doi.org/10.53347/rID-5852`. [Online; accessed 2022-06-14].

[25] U Bashir and P Rock. T2 relaxation, 2021. `https://doi.org/10.53347/rID-16494`. [Online; accessed 2022-06-14].

[26] Mimmi K Liukkonen, Mika E Mononen, Paavo Vartiainen, Päivi Kaukinen, Timo Bragge, Juha-Sampo Suomalainen, Markus KH Malo, Sari Venesmaa, Pirjo Käkelä, Jussi Pihlajamäki, et al. Evaluation of the effect of bariatric surgery-induced weight loss on knee gait and cartilage degeneration. *Journal of biomechanical engineering*, 140(4), 2018.

[27] Niels Saabye Ottosen and Hans Petersson. *Introduction to the finite element method*. Prentice Hall, New York, 1992.

[28] Matti Ristinmaa and Mathias Wallin. *Introduction to Non-linear finite element method*. Division of Solid Mechanics, Lund University, Lund, 2021.

[29] Niels Saabye Ottosen and Matti Ristinmaa. *The Mechanics of Constitutive Modeling*. Elsevier, United States, 2005.

[30] Borja Rodriguez-Vila, Patricia Sánchez-González, I Oropesa, EJ Gomez, and David M Pierce. Automated hexahedral meshing of knee cartilage structures–application to data from the osteoarthritis initiative. *Computer methods in biomechanics and biomedical engineering*, 20(14):1543–1553, 2017.

[31] FEBio software suite. FEBio User's Manual Version 2.9, 2021. `https://help.febio.org/FEBio/FEBio_um_2_9/index.html`. [Online; accessed 2022-06-04].

[32] M Henriksen, Robin Christensen, DJ Hunter, H Gudbergsen, M Boesen, LS Lohmander, and H Bliddal. Structural changes in the knee during weight loss maintenance after a significant weight loss in obese patients with osteoarthritis: a report of secondary outcome analyses from a randomized controlled trial. *Osteoarthritis and cartilage*, 22(5):639–646, 2014.

[33] Abby E Peters, Riaz Akhtar, Eithne J Comerford, and Karl T Bates. Tissue material properties and computational modelling of the human tibiofemoral joint: a critical review. *PeerJ*, 6:e4298, 2018.

[34] Andrew E Anderson, Benjamin J Ellis, Steve A Maas, Christopher L Peters, and Jeffrey A Weiss. Validation of Finite Element Predictions of Cartilage Contact Pressure in the Human Hip Joint. *Journal of Biomechanical Engineering*, 130(5), 07 2008. 051008.

[35] K Choi, Janet L Kuhn, Michael J Ciarelli, and Steven A Goldstein. The elastic moduli of human subchondral, trabecular, and cortical bone tissue and the size-dependency of cortical bone modulus. *Journal of biomechanics*, 23(11):1103–1113, 1990.

[36] JC Behrens, PS Walker, and H Shoji. Variations in strength and structure of cancellous bone at the knee. *Journal of Biomechanics*, 7(3):201–207, 1974.

[37] Babak Sarrafpour, Charbel El-Bacha, Qing Li, and Hans Zoellner. Roles of functional strain and capsule compression on mandibular cyst expansion and cortication. *Archives of Oral Biology*, 98:1–8, 2019.

[38] Dassault Systémes Simulia Corp. Hyperelastic behavior of rubberlike materials, 2017. `https://abaqus-docs.mit.edu/2017/English/SIMACAEMATRefMap/simamat-c-hyperelastic.htm`. [Online; accessed 2022-05-29].

[39] Adam A. STL to ACIS SAT conversion, 2022. `https://www.mathworks.com/matlabcentral/fileexchange/27174-stl-to-acis-sat-conversion`. [Online; accessed 2022-05-29].

[40] Paul Bolcos. Meshing Complex Geometries in Abaqus, October 2021. `https://info.simuleon.com/blog/hexahedral-meshes-for-complex-geometries-in-abaqus`. [Online; accessed 2022-05-29].

[41] Adeel Anwar, Zhenwei Hu, Yufang Zhang, Yanming Gao, Cong Tian, Xiuying Wang, Muhammad Umar Nazir, Yanfeng Wang, Zhi Zhao, Decheng Lv, et al. Multiple subchondral bone cysts cause deterioration of articular cartilage in medial oa of knee: A 3d simulation study. *Frontiers in bioengineering and biotechnology*, 8:573938, 2020.

[42] Milad Imeni, Behzad Seyfi, Nasser Fatouraee, and Abbas Samani. Constitutive modeling of menisci tissue: a critical review of analytical and numerical approaches. *Biomechanics and Modeling in Mechanobiology*, 19(6):1979–1996, 2020.

[43] Kulchamai Thienkarochanakul, Akbar A Javadi, Mohammad Akrami, Joseph Robert Charnley, and Abdelmalek Benattayallah. Stress distribution of the tibiofemoral joint in a healthy versus osteoarthritis knee model using image-based three-dimensional finite element analysis. *Journal of Medical and Biological Engineering*, 40(3):409–418, 2020.

[44] Adam C Abraham, John T Moyer, Diego F Villegas, Gregory M Odegard, and Tammy L Haut Donahue. Hyperelastic properties of human meniscal attachments. *Journal of biomechanics*, 44(3):413–418, 2011.

[45] M Khoshgoftar, ACT Vrancken, TG van Tienen, P Buma, D Janssen, and N Verdonschot. The sensitivity of cartilage contact pressures in the knee joint to the size and shape of an anatomically shaped meniscal implant. *Journal of biomechanics*, 48(8):1427–1435, 2015.

[46] Roland Becker, Sebastian Kopf, and Jon Karlsson. Loading conditions of the knee: what does it mean? *Knee Surg Sports Traumatol Arthrosc*, 21(2659–2660), 2013.

[47] David J Hunter, Grace H Lo, D Gale, Andrew J Grainger, Ali Guermazi, and Philip G Conaghan. The reliability of a new scoring system for knee osteoarthritis mri and the validity of bone marrow lesion assessment: Bloks (boston–leeds osteoarthritis knee score). *Annals of the rheumatic diseases*, 67(2):206–211, 2008.

Appendix

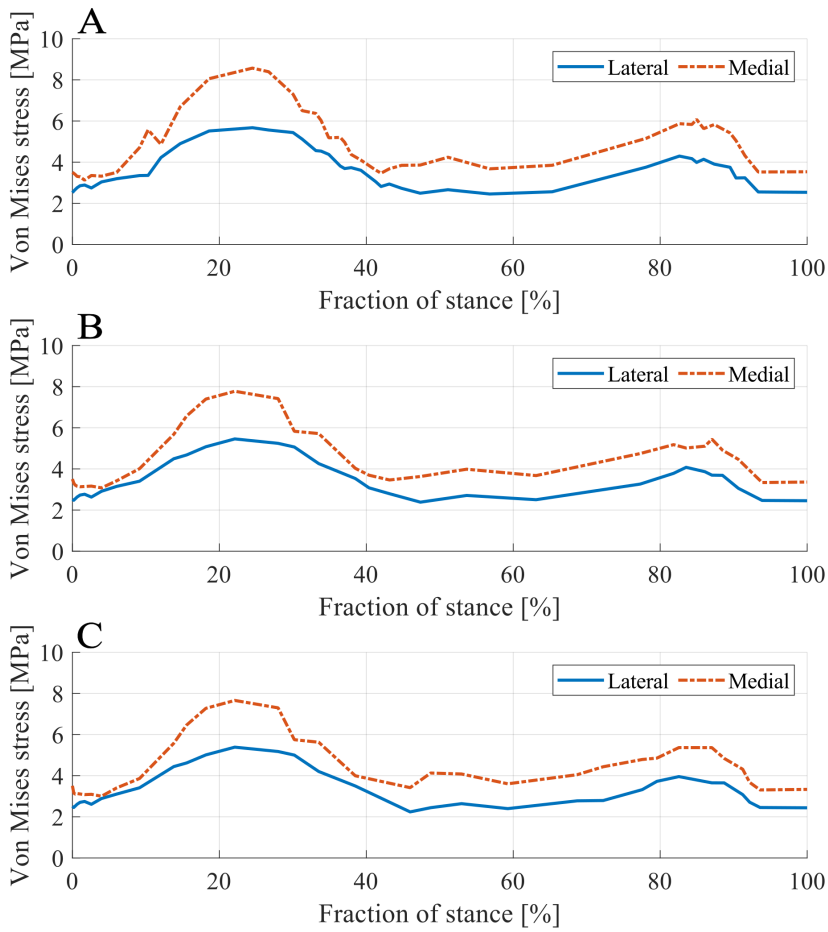

Figure 7.1: The maximum nodal Von Mises stress in the tibial cartilage at each time increment of the gait step for **A**) baseline (85 kg) **B**) 16 weeks (74 kg) **C**) 68 weeks (72 kg)

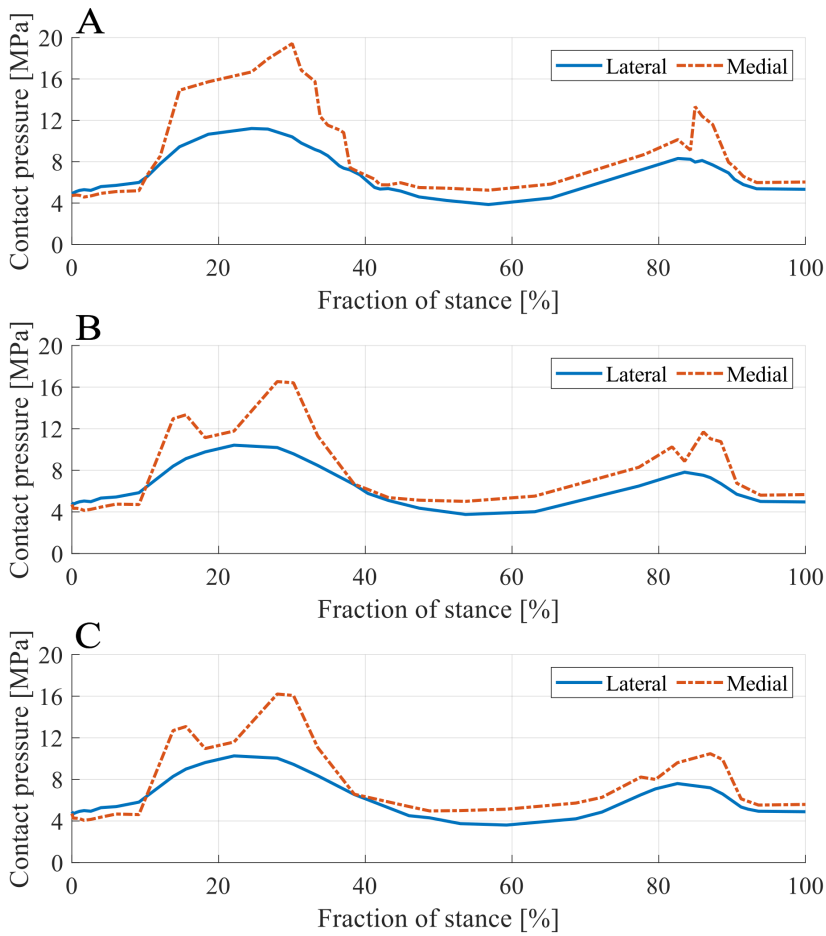

Figure 7.2: The maximum nodal contact pressure in the tibial cartilage at each time increment of the gait step for **A**) baseline (85 kg) **B**) 16 weeks (74 kg) **C**) 68 weeks (72 kg)

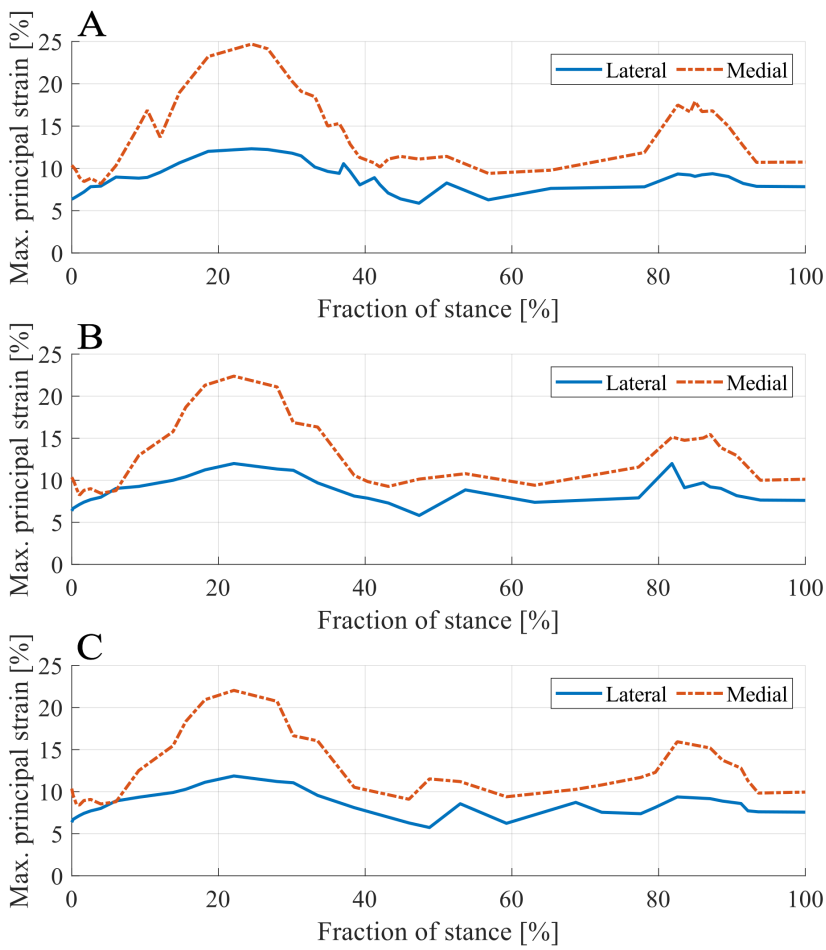

Figure 7.3: The highest nodal maximum principal strain in the tibial cartilage at each time increment of the gait step for **A**) baseline (85 kg) **B**) 16 weeks (74 kg) **C**) 68 weeks (72 kg)

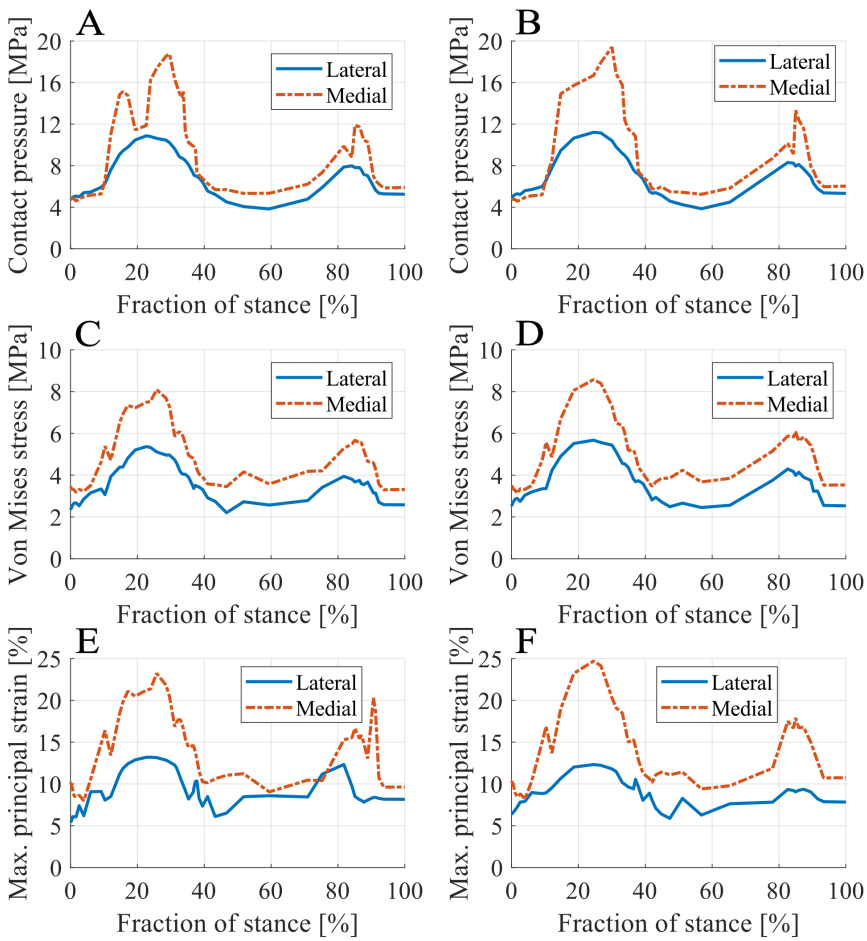

Figure 7.4: The maximum nodal contact pressure for **A**) the heterogeneous model **B**) the rigid model. The maximum nodal Von Mises stress for **C**) the heterogeneous model **D**) the rigid model. The highest nodal maximum principal strain for **E**) the heterogeneous model **F**) the rigid model.

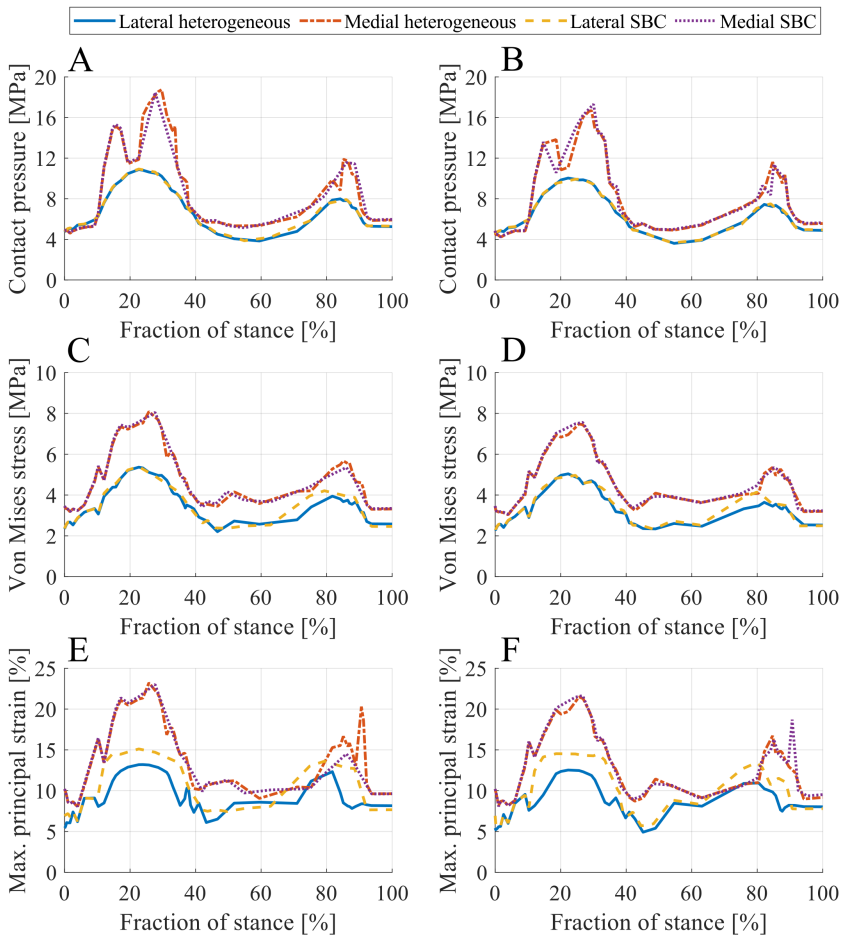

Figure 7.5: For the heterogeneous and SBC models, maximum nodal contact pressure at **A**) baseline **B**) 16 weeks. The maximum nodal Von Mises stress at **C**) baseline **D**) 16 weeks. The highest nodal maximum principal strain at **E**) baseline **F**) 16 weeks.